Open Access Dissertations   Electronic Theses and Dissertations

Enhancement of Nutrient Transport and Energy Production of the Intervertebral Disc by the Implantation of Polyurethane Mass Transfer Device

Yu-Fu Wang
University of Miami, novajason@hotmail.com

UNIVERSITY OF MIAMI

ENHANCEMENT OF NUTRIENT TRANSPORT AND ENERGY PRODUCTION OF
THE INTERVERTEBRAL DISC BY THE IMPLANTATION OF POLYURETHANE
MASS TRANSFER DEVICE

By

Yu-Fu Wang

A DISSERTATION

Submitted to the Faculty
of the University of Miami
in partial fulfillment of the requirements for
the degree of Doctor of Philosophy

Coral Gables, Florida

August 2017

UNIVERSITY OF MIAMI

A dissertation submitted in partial fulfillment of
the requirements for the degree of
Doctor of Philosophy

ENHANCEMENT OF NUTRIENT TRANSPORT AND
ENERGY PRODUCTION OF THE INTERVERTEBRAL DISC
BY THE IMPLANTATION OF POLYURETHANE MASS
TRANSFER DEVICE

Yu-Fu Wang

Approved:

_____
Chun-Yuh Charles Huang, Ph.D.
Associate Professor of Biomedical
Engineering

_____
Weiyong Gu, Ph.D.
Professor and Chair of
Mechanical and Aerospace
Engineering

_____
Fotios Andreopoulos, Ph.D.
Associate Professor of Biomedical
Engineering

_____
Alicia R. Jackson, Ph.D.
Assistant Professor of
Biomedical Engineering

_____
Howard B. Levene, M.D., Ph.D.
Assistant Professor of Clinical
Neurological Surgery

_____
Guillermo Prado, Ph.D.
Dean of the Graduate School

Low back pain is a common problem that most people experience at some point in their life. Intervertebral disc (IVD) degeneration has been considered closely associated with low back pain. Since the IVD is the largest avascular tissue in the human body, insufficient nutrient supply has been suggested to be one of the etiologies for IVD degeneration. Therefore, enhancing the nutrient transport into the IVD could be a potential treatment strategy for disc degeneration. Mass transfer devices have been used for the purpose of drug delivery and hemodialysis, and similar concept could be applied to the IVD. A porous material with high transport properties implanted in the annulus fibrosus (AF) could be designed to facilitate transport of nutrients from the edge of AF into the nucleus pulposus (NP) region. For most cellular activities in the IVD (e.g., cell proliferation and extracellular matrix production), the adenosine-5'-triphosphate (ATP) is utilized as main energy currency. ATP also serves as an important role in the formation of proteoglycan (PG) and an extracellular signaling molecule. Therefore, the overall objective of this study was to investigate the relationship between porosity and mass transport and mechanical properties of porous polyurethane (PU) scaffolds, as well as the enhancement of nutrient transport and ATP production in the IVD by the implantation of porous PU scaffolds in the AF as mass transfer devices.

The mechanical and mass transport properties of porous PU scaffolds fabricated by the combination of phase inversion and salt leaching method were systematically characterized, and its relationships with porosity were investigated. The results demonstrated that porosity could be utilized to govern both mass transport and mechanical properties of porous scaffolds. The relationships could facilitate the porous PU scaffolds fabrication with specific mass transport and mechanical properties. The effect of implantation of PU mass transfer devices in the IVD was studied. The results demonstrated that compressive stiffness and the height of the IVD could be preserved with the implantation of the devices. The level of ATP, lactate and PG was also found to be increased in the device group. The results indicated that implantation of the PU mass transfer devices could promote nutrient transport and enhance energy production without compromising the mechanical and cellular functions in the IVD. In the last section, the theoretical model of mechano-electrochemical mixture theory was validated using the organ culture of porcine IVD, and different designs of mass transfer device were also theoretically analyzed. The results demonstrated good agreement between experimental and theoretical glucose distribution. In addition, the larger size of the mass transfer device and device with impermeable AF portion could also enhance the glucose concentration and consumption rate at the NP region. The findings of this dissertation contribute to further understanding the effect of implantation of PU mass transfer device in the IVD, and the results could help the development of novel treatment strategies for IVD degeneration and low back pain.

Acknowledgment

First, I would like to express my special appreciation and thanks to my advisor Dr. Chun-Yuh Charles Huang, you have been a tremendous mentor for me. I would like to thank you for encouraging my research and for allowing me to grow as a research scientist. Your advice on both research as well as on my career have been priceless.

I would also like to thank my committee members, Dr. Weiyong Gu, Dr. Alicia R. Jackson, Dr. Fotios Andreopoulos and Dr. Howard B. Levene. Thank you for sharing your expertise and offering valuable advice to this work and the time you kindly spent serving on my committee.

Special thanks to the Stem Cell and Mechanobiology Lab members: Chong Wang, Lauren Vernon, Daniella Gonzales, Amaris Genemaras, Xue Yin and other undergraduates working in the lab. Thank you all for offering me great advice and help on research and daily life starting from my first day entering the lab. I would also like to thank my friends from other labs: Xin Gao, Qiaoqiao Zhu, Kelsey Kleinhans and Lukas Jaworski etc. Without the help from all of my friends, I would not able to finish my Ph.D. works.

Lastly and most importantly, A special thanks to my family. Words cannot express how grateful I am to my parents and my older sister for all of the sacrifices that you've made on my behalf. Without the supporting from my family, I would not have accomplished my goals.

Table of Contents

List of Figures

List of Tables

Chapter 1: Introduction and Specific Aims

1.1 Introductory Remarks

Low back pain affects up to 85% of people in their lifetime. This contributes to healthcare costs in the United States which exceeds $100 billion per year [1, 2]. One of the major causes of low back pain is believed to be related to the degeneration of the intervertebral disc (IVD) [3, 4]. The IVD is the largest avascular tissue in the human body, and insufficient nutrient supply has been suggested as one of the etiologies for disc degeneration [5, 6]. There are two major pathways for nutrient transport into the IVD [7, 8]. The annulus fibrosus (AF) receives nutrients from capillaries in the soft tissues that surround at the edges of the AF [9, 10]. The vertebral blood vessels are the main nutrient sources for the central region of the IVD, nucleus pulposus (NP) [11, 12]. The exchange of nutrients and metabolites in the IVD are mainly driven by the concentration gradient [13]. This results in the central region of the IVD having lower levels of oxygen and glucose and other nutrients compared to the outer region [14, 15]. As long as the nutrient levels remain above a vital threshold, the viability and functionality of the IVD can be maintained. When the nutrient demand exceeds supply, it results in decreased cellular activity levels and may ultimately cause cell death [16-18]. For example, calcification of the endplate with aging causes a reduction in the nutrient level in the NP region [19-21] which is detrimental to cellular function such as extracellular matrix (ECM) production and may consequentially lead to disc degeneration. Therefore, addressing and supplementing nutrient supply could be one of the potential treatment strategies for treating or reversing disc degeneration.

Most of the cellular activities in the IVD such as ECM production and maintenance are high energy demanding processes which require adenosine-5'-triphosphate (ATP) as fuel [22]. ATP also serves as a building block in the formation of UDP-sugars and 3'-phosphoadenosine 5'-phosphosulphate for biosynthesis of proteoglycans (PG) [23, 24] which is one of the major ECM components in the IVD. In addition, ATP is an extracellular signaling molecule that mediates a variety of cellular activities through purinergic signal pathways [25-27]. Our previous study demonstrated that mechanical loading promotes ATP production and release in IVD cells [28] while extracellular ATP can modulate the ECM biosynthesis of IVD cells [29]. Therefore, under the malnourished condition, the metabolism of ATP in the IVD may play an important role in maintaining the integrity and function of the IVD.

The utilization of mass transfer devices (e.g., microporous catheters) for drug delivery and hemodialysis has been shown in previous studies [30-33]. The purpose of the devices is to remove cellular metabolic waste and deliver therapeutic compounds to body based on the principle of diffusion of solutes across a semi-permeable membrane. A similar concept could be applied in the IVD. In addition, implantation of biomaterials for closure of the AF to maintain the height and stability of the IVD has been shown in previous studies [34-36]. Since there are ample nutrient supplies at the edges of the AF due to blood circulation, porous materials implanted in the AF may facilitate transport of nutrients from the edge of the AF into the NP region and also have the possibility to preserve the stability of the IVD. Therefore, the objective of this study was to investigate the relationship between porosity and mass transport and mechanical properties of porous PU scaffolds, and to investigate the enhancement of nutrient transport and energy

production in the IVD by the implantation of porous PU scaffolds in the AF as a mass transfer device.

1.2 Specific Aims

The following are the hypotheses of this study:

1. The mechanical and transport properties of PU scaffolds are functions of porosity.

2. Implantation of PU mass transfer devices facilitates the nutrient transport and energy production in the IVD.

To test the hypotheses, the following are the specific aims of this project.

Aim 1: To investigate the mass transport and mechanical properties of the porous PU scaffolds and their relationship with porosity

The porous PU scaffolds were fabricated by the phase inversion and the salt leaching method. The tensile and compressive moduli of PU scaffolds were examined with different PU concentration and salt/PU weight ratios. In addition, the mass transport properties, including hydraulic permeability and glucose diffusivity, were also measured. Furthermore, the relationships between porosity and mass transport and mechanical properties of porous PU scaffolds were systemically investigated. Statistical analysis tools were used to determine the significant differences in mechanical and transport properties among experimental groups.

Aim 2: To investigate the enhancement of ATP production in the IVD by the implantation of PU mass transfer devices

The porcine functional spine units (FSUs) were isolated and divided into intact, device and surgical groups. For the device and surgical groups, two puncture holes were created bilaterally at the dorsal side of the AF region without removing tissue. The PU mass transfer devices were squeezed and implanted under a press-fit condition in the device group only. After 7 days of culture, the mechanical testing, including disc height reduction and compressive stiffness, were examined. In addition, glucose distribution, cell viability, ATP, lactate, PG and DNA content were also tested. The mechanical and biological effect of implantation of PU mass transfer devices were systemically investigated. Statistical analysis tools were used to determine significant differences among experiment groups.

Aim 3: To validate the theoretical model of the mechano-electrochemical mixture theory using the organ culture of porcine IVD and theoretically analyze different designs of the PU mass transfer device

The porcine FSUs were divided into intact and device groups. Two puncture holes were created at the dorsal side of the AF region in the device group, and the PU mass transfer devices were inserted under press-fit condition. The glucose distribution was measured after 7 days of culture. The experimental glucose distribution was compared with simulation results from the theoretical model which were based on the mechano-electrochemical mixture theory. Furthermore, different designs of the mass transfer device were also analyzed by the theoretical model. The glucose concentration and

consumption rate of different sizes of mass transfer devices and a device with impermeable AF portion were investigated.

1.3 Structure of Dissertation

The overall objective of this research was to investigate the relationships between porosity and mass transport and mechanical properties of porous PU scaffolds, and the utilization of porous PU scaffolds as mass transfer devices for the augmentation of energy production and nutrient transport in the porcine IVD. A background of IVD, disc degeneration, importance of ATP and PU application was given in chapter 2. To achieve the objective of this study, the porous PU scaffolds were fabricated by the phase inversion and the salt leaching method in chapter 3. The mechanical properties including tensile and compressive moduli were measured, and the hydraulic permeability and the glucose diffusivity were also determined. The relationships between porosity and mechanical and mass transport properties were described. In chapter 4, the effect of implantation of PU mass transfer devices in the porcine IVD were investigated. After 7 days of culture, the overall structure properties of FSUs were measured. The biological measurement, including glucose distribution, cell viability, ATP, lactate, PG and DNA content, were also examined. In chapter 5, validation of glucose distribution between theoretical simulation and experimental results was described. In addition, different designs of PU mass transfer device were analyzed by the theoretical model. In Chapter 6, the major findings of this study were summarized and the recommendation for the future work were also presented.

Chapter 2: Background and Significance

2.1 Characteristics of Intervertebral Disc

The IVD consists of multiple and structurally distinct anatomical regions which include AF, NP and cartilaginous endplates (CEP) [37]. The central gel-like NP is peripherally contained by the AF and the IVD is sandwiched between two units of CEPs connected to adjacent vertebrae as shown in Figure 2-1 [7, 38]. Each of the tissues has a different function and is consisted of a specific matrix structure that is maintained by a distinct cell population. The NP is predominately made up of water (70% to 90%, depending on the age), collagen type II (20% of dry weight) and PGs (50% of dry weight) [7]. The large quantities of PG in the NP region aggregate along chains of hyaluronan (Figure 2-2) [39, 40]. The glycosaminoglycan side chains of these PGs carry fixed negative charges and generate an osmotic swelling pressure within an irregular meshwork of collagen II fibrils [41]. The AF is made up of 15-25 concentric lamellae, with the collagen fibers lying parallel within each lamella. The fibers are orientated at approximately 60° to the vertical axis, alternating to the left and right of its adjacent lamellae (Figure 2-3) [42]. The composition of the AF includes water (60% to 80%, depending on age), collagen (50% to 70% of dry weight), PGs (10% to 20% of dry weight) and non-collagenous protein (25% of dry weight) [7]. The proportion of type I collagen increases from the inner AF to the outer AF, whereas type II collagen follows an inverse distribution [8]. The different composition explains that these two regions endure different kinds of stress. Collagen can provide firmness and tensile strength. On the contrary, when PG interacts with water, it provides the tissue stiffness and resists compression stress. Therefore, the AF region is primarily responsible for withstanding

www.manaraa.com

tensile stress and the NP region is for compressive stress [5, 43]. With these special stress endurance structures, the IVD can sustain a large amount of loading. The human lumbar disc can endure pressure around 0.2 MPa in a lying down position [44]. The stress will increase 3 to 5 fold when we change posture or perform movements [38].

The developmental origin of the AF and the NP are different. The annulus derives from the mesenchyme and the nucleus derives from the notochord. In early human childhood, notochordal cells are found in the NP region, and their phenotype and function have an important role in the NP development. The number of notochordal cells decreases rapidly and disappears during early adulthood for an unclear reason [45]. Compared to notochordal cells, mature NP cells are smaller, rounded and lack intracellular vacuoles. There is increasing evidence indicating that mature NP cells are derived from the notochordal cells [43, 46-48]. The density and phenotype of IVD cells vary with different species. In general, the cell density of the human disc decreases with age and varies with region. At maturity, the human cell density of the NP is about 4000 cells/mm^3 and that of the AF is about 9000 cells/mm^3 [49].

2.2 IVD Degeneration and Nutrients Supply

The etiology of the IVD degeneration is still unclear but has been suggested to be associated with mechanical loading, genetic predisposition and nutrient supply [8, 43, 50]. The correlation between mechanical loading and disc degeneration in clinical studies and animal experiments are not completely conclusive. The majority of animal studies suggest that certain forms of mechanical loads could induce disc degeneration.

(a)

(b)
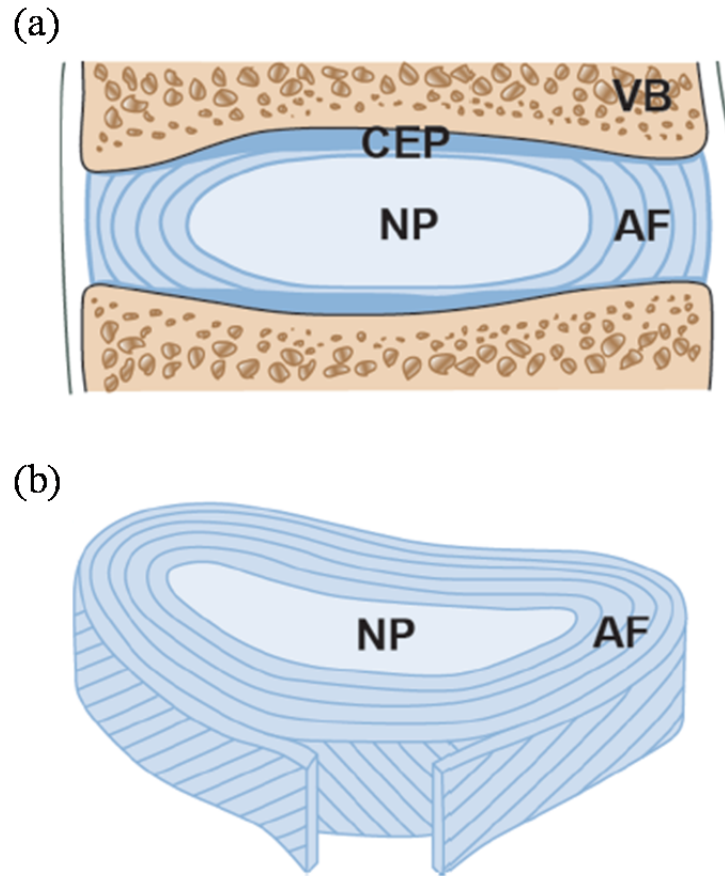
Figure 2-1. (a) Schematic representation of the IVD which is sandwiched by the cartilaginous endplate (CEP) and vertebrae (VB). (b) Schematic showing the layered structure annulus fibrosus (AF) which encapsulate the central nucleus pulposus (NP). [7]
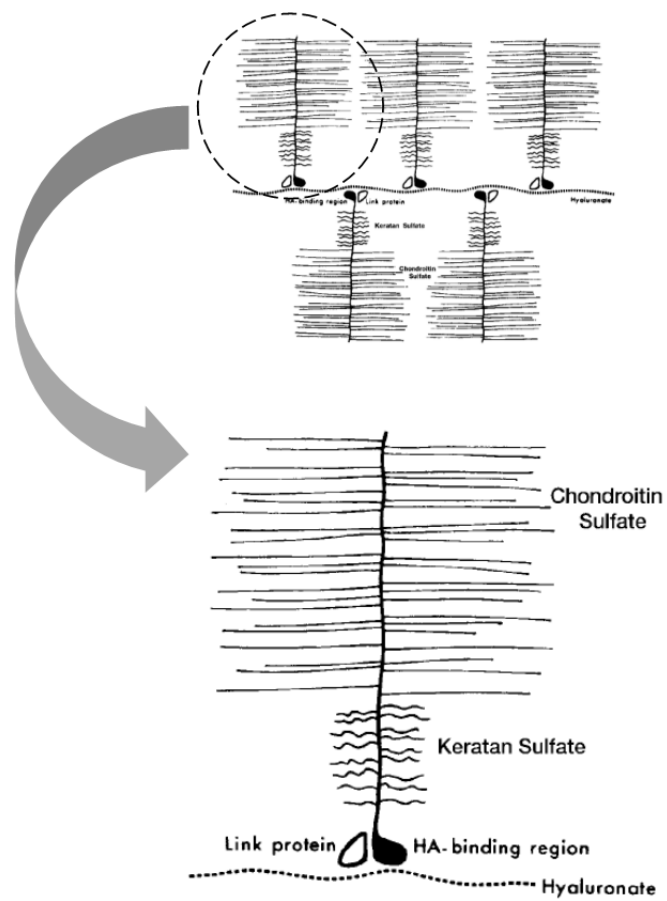
Figure 2-2. Schematic view of a proteoglycan unit. [39]
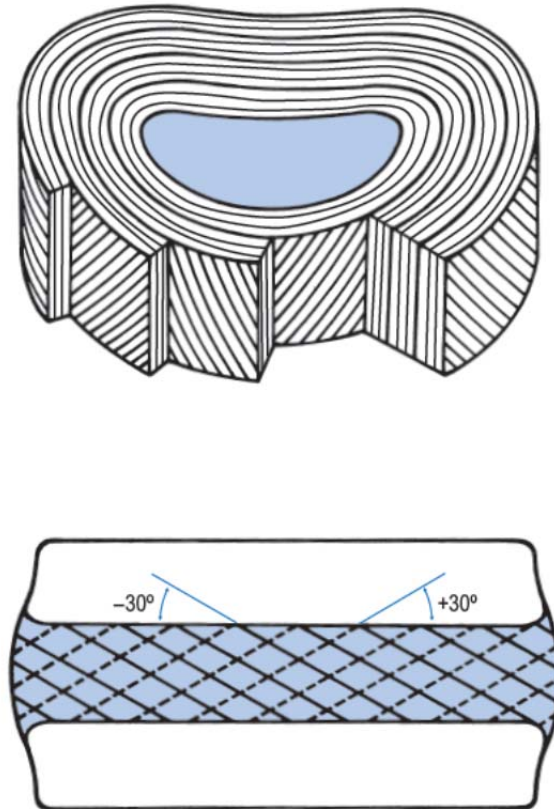
Figure 2-3. Schematic view of AF structure. The fibers are orientated at approximately 60° to the vertical axis and alternating to the left and right of it in adjacent lamellae. [42]

However, in human studies, the strong link between mechanical factors (e.g., heavy physical work or lifting) and disc degeneration have failed to be proven which suggests a more complex etiology of IVD degeneration [50]. Besides the mechanical loading, several studies have demonstrated a strong familial predisposition for disc degeneration. The results from twin studies have suggested that overall heritability of disc disease at lumbar spine is between 52% to 74% [51, 52]. The genetic effects have been believed to be one of the important factors in disc degeneration [50]. Although genetic factors seem strongly involved, insufficient nutrient supply has also been suggested as one of the factors due to the avascular nature of the IVD [10].

As mentioned in the previous chapter, there are two major nutrient transport pathways into the IVD: one is through the peripheral AF route and the other is through the CEP route (Figure 2-4a). The outer AF region can receive nutrients from capillaries in the soft tissue that surrounds the disc. The central NP and the inner AF region which are far from the surrounding soft tissue capillaries need the nutrients transported from the vertebrae vessels [9]. The vertebrae blood vessels penetrate the marrow space and subchondral bone and form the loop near the CEP [11, 48]. The nutrients from the vertebrae blood vessels diffuse through the CEP to the central region of the IVD by the concentration gradient, whereas the metabolites diffuse out in an opposite direction [13]. Therefore, the central region of the IVD has lower levels of oxygen, glucose and other nutrients compared to the outer region (Figure 2-4 b) [14, 15]. The defect of the nutrient supply to the IVD, such as impaired vertebral or CEP blood supply, might decrease cell activity level, cause cell death and result in disc degeneration. The impaired vertebral blood supply might be due to the atherosclerosis of the arteries that feed the lumber spine or to

(a)

(b)
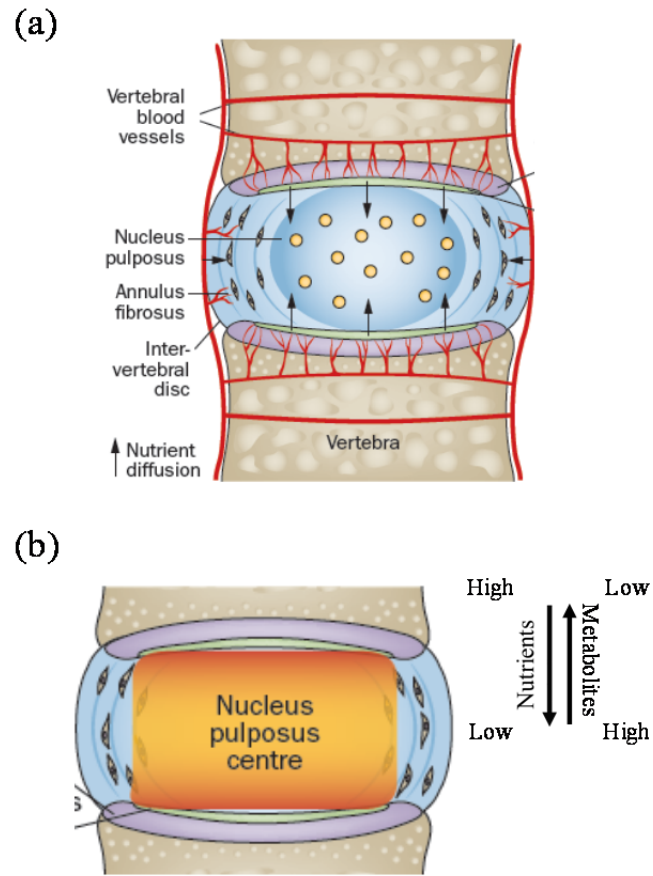
Figure 2-4. Schematic view of (a) IVD nutrients supply pathways and (b) nutrients and metabolites distribution. [17]

disorders such as Gaucher disease, sickle cell anaemia and Caisson disease which negatively affect the microcirculation. Alternatively, the impaired CEP blood supply might be due to the occlusion of the marrow spaces or the calcification of the CEP which results in losing the contact between the capillaries and the CEP or inhibiting diffusion of solutes from capillaries to the disc respectively [17]. The importance of the CEP route for solutes transport into IVD has been demonstrated in previous *in vivo* animal studies. The diffusion of hydrogen molecules was measured at the NP region in adult mongrel dogs and the reduction was found when the CEP route was disrupted [53]. The magnetic resonance imaging study with contrast agent gadodiamide injection in humans also showed that CEP route played an important role in IVD degeneration [54]. One can observe that IVD degeneration is strongly associated with the defect of nutrients supply.

2.3 Characteristics of IVD Degeneration

IVD degeneration is believed to start as early as the second decade of life which is earlier than other connective tissues such as bone, tendon and ligament [55, 56]. With increasing of age, as growth and skeletal maturation proceeds, the degenerative process starts to change the morphology and the function of the disc. This is also reflected in the changes in the biosynthesis and denaturation of the ECM during the progressing age. The NP of degenerated disc showed decreased water and PG contents which leads to less gel-like appearance and hydrostatic properties. Degenerative changes of the AF are less obvious but result in irregular lamellae with the collagen and elastin network becoming more disorganized [50] (Figure 2-5). The most significant biomechanical change to occur
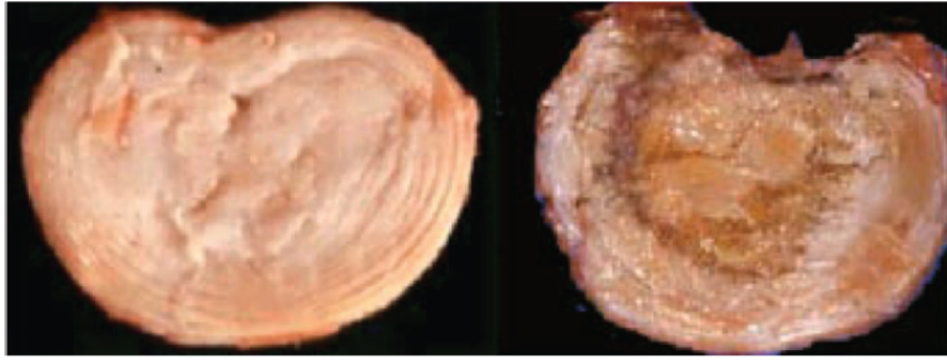
Figure 2-5. The normal (left) and degenerated (right) human lumber IVD. The degenerated disc showed desiccated NP and disorganized AF when comparing to the normal disc. [8]

in disc degeneration is the loss of PG. The aggrecan molecule becomes degraded, with smaller fragments being able to leach from the tissue more readily than the larger protein. The loss of glycosaminoglycan is responsible for a fall in the osmotic pressure of the disc matrix and the loss of hydration [8].

2.4 Intervention of IVD Degeneration

The primary interventions for disc degeneration are conservative and surgical treatments [57]. For the conservative approach, rehabilitation programs and lifestyle adjustment such as weight loss are suggested to patients. However, a previous study shows that surgical treatment has a better outcome compared to the conservative treatments [58]. Spinal fusion re-raises the degenerated disc, but also has a significant downside. The flexibility between the fused vertebrae will be eliminated. This causes the stress and strain on the adjacent discs to increase and this accelerates their degeneration [43, 59]. Disc arthroplasty is the surgery that involves replacing the original degenerated disc with an artificial disc. However, it has the potential for displacement and component failure [59, 60].

The biological approach is another growing research area for IVD degeneration treatment. Recent small animal studies on emerging biological therapies of disc degeneration have shown promising results [57, 61]. For example, since several growth factors (e.g., TGF-β, IGF-1, BMP) are known to up-regulate the anabolic activity of disc cells [62-65], exogenous administration of growth factors has been proposed as a potential therapy for disc degeneration [63-65]. Besides growth factors, transplantation of stem cells or differentiated cells also showed promising results [57]. Both biological

approaches increase cell nutrient demand. Growth factors promote cell proliferation and ECM production [63, 66], and cell transplantation enlarges the original nutrient consumption [44]. However, the problem of greater nutrient restriction might appear in larger animal models, e.g. porcine, due to bigger disc size and larger diffusion distance. With lower nutrient diffusion supply, the effectiveness of a cell based treatment might decrease [57].

2.5 Importance of ATP in the IVD

Most cell activities in the IVD, such as ECM production and maintenance, are high energy demanding processes which require ATP as fuel [29, 30]. ATP is so-called the molecular unit of currency which can be hydrolyzed into adenosine diphosphate and adenosine monophosphate [67, 68]. In the production of ATP, glycolysis is the process by which cells break down glucose into pyruvate and produce ATP. When pyruvate enters the mitochondria, more ATP is produced by the Krebs cycle and the electron transport in aerobic condition. On the other hand, pyruvate is oxidized into lactate without ATP production in anaerobic condition [14, 19, 48]. Due to the avascular nature of IVD, ATP is predominantly believed to be generated by the glycolysis pathway in the IVD [31, 32]. ATP also serves as a building block in the formation of UDP-sugars and 3'-phosphoadenosine 5'-phosphosulphate for biosynthesis of PGs [23, 24] which are one of the major ECM components in the IVD. Furthermore, ATP is an extracellular signaling molecule that mediates a variety of cellular activities. It can regulate the cell metabolism, survival and growth through purinergic signal pathways [33-35]. Our previous studies also demonstrated that mechanical loading promotes ATP production

and releases from IVD cells, and the extracellular ATP enhanced the ECM production of IVD cells, suggesting that ATP could regulate the IVD metabolism [28, 29]. During disc degeneration, nutrient (e.g. glucose and oxygen) diffusion in the IVD is decreased which could affect the glycolysis pathway and could lead to the reduction of ATP. Therefore, ATP in the NP region might play an important role in maintaining a healthy ECM structure of the IVD.

2.6 Porous Polyurethane Scaffold

For years, polyurethane (PU) has been extensively used in various implantable devices such as catheters, pacemaker leads, intra-aortic balloons and mammary implants [69, 70]. The in vivo molecular stability of PU provides a successful clinical utilization [71]. And for the last several years, porous PU scaffold has become one of the most popular biomaterials in tissue engineering fields, such as small diameter vascular grafts, cartilage, and bone tissues [72-79]. In the previous studies, the porous PU formations have been introduced by several methods. For example, Wang et al. produced the small diameter vascular graft by the electrospun method [74], Khorasani et al. employed the phase inversion technique to form the vascular graft [75], Whatley et al. used the freeze-dried process to fabricate the PU scaffold for the IVD application [76], Hung et al, developed a 3D printing method with PU for the cartilage tissue engineering [77], and the combination of the phase inversion and porogen leaching methods were also utilized to form porous scaffold by Levene, Gorna et al. and Heijkants et al. for both bone and cartilage tissue engineering [78-80]. Sodium chloride (NaCl) is one of the most common particles used as the porogen in the particle leaching method [81]. The size and amount of

NaCl can be controlled as parameters to adjust the porosity of the scaffold. One of the key challenges in porous scaffold design is to create a porous structure with desired mechanical function and mass transport properties which aids delivery of biofactors and the development of functional tissue substitutes [82].

2.7 Significance of This Study

Disc degeneration is believed to be associated with low back pain which affects millions of people in the US. Due to the avascular nature of the IVD, essential nutrients are delivered by diffusion and convection through dense ECM over a long distance to the NP region from the blood supply at either the margin of the AF or the vertebrae. In addition, poor nutrient supply has been considered to be one of the factors in IVD degeneration. ATP is the molecule which is required for high energy demanding cell activities, and it also serves as an extracellular signaling molecule. Our previous studies suggested that ATP production may play an important role in maintaining healthy ECM structure of the IVD [28, 29]. The utilization of mass transfer devices has been demonstrated for drug delivery and hemodialysis. However, no studies have been conducted to investigate the effects of mass transfer devices on nutrient transport in the IVD. Therefore, the overall objective of this study was to investigate the relationship between porosity and mass transport and mechanical properties of porous PU scaffolds, as well as the enhancement of nutrient levels and ATP production in the IVD by the implantation of porous PU scaffolds in the AF as mass transfer devices. The results of this study will help the development of potential treatment strategies for disc degeneration.

Chapter 3: Systematic Characterization of Porosity and Mass Transport and Mechanical Properties of Porous Polyurethane Scaffolds

3.1 Introductory Remarks

For years, PU has been extensively used in various implantable devices such as catheters, pacemaker leads, intra-aortic balloons and mammary implants [69, 70]. The in vivo molecular stability of PU provides a successful clinical utilization [71]. In recent years, porous PU scaffolds have become one of the most popular biomaterials in various tissue engineering applications, such as in small diameter vascular graft and regeneration of cartilage and bone tissues [72-79]. Formation of porous PU scaffolds has been achieved by several methods, such as electrospinning, phase inversion and porogen leaching [74-79]. One of the key challenges in porous scaffold design is to create a porous structure with desired mechanical function and mass transport properties which aid delivery of biofactors and development of functional tissue substitutes [83].

The mechanical properties (Young's modulus in tension and compression) of PU scaffolds have been characterized for their specific applications. The tensile modulus of PU has been examined for the small diameter vascular graft application because of the need of resisting pressure from blood flow [84]. With different formation methods with and without wall reinforcement, the tensile modulus requirement for small diameter vascular grafts ranged from 0.05 MPa to 4 MPa [74, 75, 83, 85]. In the application of cartilage and bone tissue engineering, the porous PU scaffolds are utilized as a temporary ECM and also provide a sufficient mechanical strength to withstand in vivo stress and loading [86]. With various fabrication methods and modification, the compressive moduli of PU scaffolds for cartilage tissue engineering usually ranged from 0.01 MPa to 1 MPa

[69, 76, 77, 79, 87, 88]. Because of different mechanical characteristics between cartilage and bone tissues, PU scaffolds for bone tissue engineering have higher compressive moduli which range from 2.5 MPa to 50 MPa [89, 90]. Therefore, creating scaffolds with adequate mechanical properties is important for various applications.

Mass transport properties (e.g., permeability and diffusivity) of porous scaffolds are also important in maintaining cell health by facilitating exchanges of nutrients and metabolites for tissue engineering applications. Transport of fluid and solutes within porous scaffolds is mainly affected by their hydraulic permeability and solutes diffusivities [91, 92]. Hydraulic permeability represents a measurement of how easy the fluid can flow through a porous material, while diffusivity is a measurement of solute mobility. Therefore, fully understanding the mass transport properties of porous scaffolds is necessary for successful tissue engineering applications.

Previous studies have showed that permeability and solute diffusivity were highly dependent upon porosity in tissues and scaffolds [92-94]. Furthermore, it has also been demonstrated that scaffold porosity is strongly associated with mechanical properties [94-101]. Although high porosity is desirable for efficient transport of nutrients in the scaffolds for tissue engineering applications, it reduces the mechanical properties of the scaffolds. Therefore, seeking the balance between efficient mass transport and sufficient mechanical strength is one of the challenges in the scaffold design. By understanding the relationships between porosity and mass-transport and mechanical properties, it allows us to facilitate the design of porous scaffolds with desired mass transport and mechanical properties for tissue engineering applications. However, the relationship between porosity and both mass transport and mechanical properties of PU porous scaffolds have not been

fully elaborated. Therefore, the objectives of this study were to systemically investigate the mass transport and mechanical properties of the porous PU scaffolds and their relationship with porosity.

3.2 Materials and Methods

PU Scaffold Preparation

The PU solution was prepared by dissolving PU pellets (Tecflex® SG-85A, Lubrizol, Wickliffe, OH,) in the N,N-dimethyl formamide (DMF; Sigma-Aldrich, St. Louis, Mo., USA) with 25%, 20% and 15% (w/v) concentration, respectively. Porous PU scaffolds were prepared using a sodium chloride (NaCl; Sigma-Aldrich) salt-leaching method. NaCl crystals were grinded, sieved to sizes smaller than 75 µm and mixed into the PU solution at three different weight ratios (NaCl/PU ratio: 9/1, 6/1 and 3/1). Polytetrahydrofuran (Sigma-Aldrich) was added to the NaCl/PU mixture in 25% (v/v) volume ratio as a soluble filler to enhance interconnectivity in PU scaffolds [102]. The mixed solution was well stirred and then injected into a plastic rectangular mold. After injection, the mold was placed at room temperature for two hours to evacuate air bubbles and then stored at -80◦ C overnight to solidify PU resin. The frozen PU resin was

removed from the mold and merged in 65% of ethanol with 1% DMF solution for phase inversion process for 24 hours. The porous PU scaffolds were then rinsed in distilled water for another 24 hours in order to remove remaining NaCl crystals. After the rinse procedure, PU samples were punched in different sizes for the further analyses of mechanical and mass transport properties. Three independent tests were performed for each experimental group in each analysis. Samples were freshly prepared for individual

tests and were not reused for different tests.

Porosity

To measure porosity, PU samples were air dried and punched into cubic shape (n=3 per NaCl/PU ratio or PU concentration). The length and mass of samples were measured with a digital caliper and scale, respectively. The porosity was calculated by the volume and mass of the sample with the following equation [79]:

$$\varphi = 1 - \frac{\rho}{\rho_{polymer}} \tag{1}$$

Where φ was the porosity, ρ was the density of the porous PU scaffold and the $\rho_{polymer}$ is the density of the pure polymer.

Scanning Electron Microscopy (SEM)

25% PU samples with different NaCl/PU ratios were prepared (n=3 per NaCl/PU ratio) and the mid-height cross section area of the samples were scanned under the SEM (JSM-6010PLUS/LA, JEOL, Peabody, MA) at the acceleration voltage 1.5Kv. Three random locations of each ratio groups were captured for pore size and distribution measurement by ImageJ software. The Saltykov theory was utilized as a stereology analysis for the estimation of 3D pore size distribution [103, 104].

Mechanical Properties

PU samples were prepared in cuboid shape (25mm x 15mm x 3mm, n=3 per NaCl/PU ratio or PU concentration) for tensile testing which was performed using a single column testing system (Instron, Norwood, MA). With a 5% tensile strain preload, the PU samples

were subjected to 10% strain and tensile load was measured after 500 seconds of relaxation. For compressive testing, the PU samples were prepared in cylindrical shape (diameter: 5.8mm, height: 3mm, n=3 per NaCl/PU ratio or PU concentration) using a punch. Compressive testing was performed using a custom-made loading system [28] which consisted with a stepper motor (Moog Animatics, Santa Clara, CA) and a high accuracy low profile load cell (OMEGA Engineering Inc., Stamford, CT). Similarly, 5% of compressive strain was used as a preload and compressive load was measured after application of 10% strain with 500 seconds of relaxation. Young's moduli of PU samples in tension and compression were determined and normalized by that of the scaffold fabricated with phase inversion method only. The relationship between porosity and normalized Young's modulus was determined by the following equation [98]:

$$E = c(1 - \varphi)^\alpha \tag{2}$$

where c and α are the material parameters, φ is the porosity and E is the normalized Young's modulus in either tension or compression. The material parameters were curve fitted by MATLAB software (MathWorks Inc., Natick, MA).

Hydraulic Permeability

PU samples were prepared in cylindrical shape (diameter: 7.8mm, height: 1mm, n=3 per NaCl/PU ratio) and the measurement of hydraulic permeability was performed as described in our previous study [105]. Briefly, the PU samples were placed between two compartments in a permeability chamber. By creating a pressure gradient across the PU sample with phosphate-buffered saline (PBS) solution, the hydraulic permeability can be determined by Darcy's law:

$$k = \frac{Q\,h}{A\,\Delta P} \tag{3}$$

Where k is the hydraulic permeability, Q is the volume flow rate, h is the thickness of the sample, A is the effective cross section area of the sample and ΔP is the pressure gradient across the PU sample. The relationship between hydraulic permeability and porosity was determined by the following equation [106, 107]:

$$k = \beta\left(\frac{\varphi}{1-\varphi}\right)^{n} \tag{4}$$

where β and n are the material parameters. And the material parameters were determined by curve fitting with MATLAB.

Glucose Diffusivity

PU samples were prepared in cylindrical shape (diameter: 5.8mm, height: 1mm, n=3 per NaCl/PU ratio) and the measurement of glucose diffusivity was performed as described in our previous study [108]. Briefly, the PU samples were placed between two compartments in a diffusion chamber. PBS solutions with and without 20 g/L glucose were injected into the upstream and downstream compartments, respectively. Glucose concentration in the downstream compartment was measured using an optical glucose probe that was fabricated by encapsulated glucose oxidase in the enzyme layer of the optical sensor described in our previous study [109]. The glucose diffusion coefficient was calculated by the following equation [108]:

$$D = \ln\left[\frac{C_{up}-C_{down}(t_0)}{C_{up}-C_{down}(t)}\right]\frac{V_{down}h}{A(t-t_0)} \tag{5}$$

where D is the glucose diffusivity in the sample, C_{up} was the glucose concentration in the upstream compartment, C_{down} was the glucose concentration in the downstream

compartment, V_{down} is the volume of solution of downstream chamber, A is the diffusion area and h is the thickness of the sample. $C_{down}(t_0)$ and $C_{down}(t)$ are the concentration of glucose in the downstream chamber at initial time t_0 and t, respectively. The relationship between the glucose diffusivity and porosity was descried by the following equation [110]:

$$\ln\left(\frac{D}{D_0}\right) = \left[-a\left(\frac{1-\varphi}{\varphi}\right)^b\right] \tag{6}$$

where D_0 is the glucose diffusivity in the water (9.4×10^{-6} cm^2/s) and a and b are material constants. The material constants were determined by curve fitting with MATLAB.

Statistical Analysis

Differences in transport and mechanical properties among experimental groups were analyzed by one-way ANOVA, followed by LSD post-hoc test. The p-value < 0.05 was considered significant.

3.3 Results

Effects of salt incorporation on pore size and porosity of PU scaffolds

The pure PU scaffolds produced only by the phase inversion method contained small pores (4.5~10µm) (Figure 3-1; Table 3-1). The salt leaching method created sponge-like PU scaffolds with a randomly distribution of larger pores in addition to small pores. Based on the analysis of pore size distribution, the majority of pore size was found between 30 and 50 µm (Figure 3-1c). With higher NaCl/PU weight ratios, more porous PU scaffolds were produced. The porosity of the PU scaffolds significantly increased with increasing NaCl/PU weight ratio (Figure 3-2a). The average porosities of all samples fabricated with three different PU concentrations were 68.81±1.723%, 61.07±2.78% and 28.38±5.68% for the NaCl/PU weight ratio of 9/1, 6/1 and 3/1, respectively. The relationship between the scaffold porosity and NaCl/PU weight ratio can be described by the following equation (Figure 3-2b):

$$\varphi = -2.799x^{-1.586} + 0.774 \ (R^2 = 0.96) \tag{7}$$

where x is the NaCl/PU ratio (x range from 2.5 to 10). Furthermore, the porosity and pore size were not affected by the original PU concentration (Figure 3-2)

Table 3-1. The average pore sizes of 25% PU scaffolds with different NaCl/PU weight ratios.

NaCl/PU Weight Ratios	Average Pore Sizes (µm)
9/1	39.743±10.76
6/1	40.690±11.98
3/1	42.324±12.10
0/1	6.819±1.28
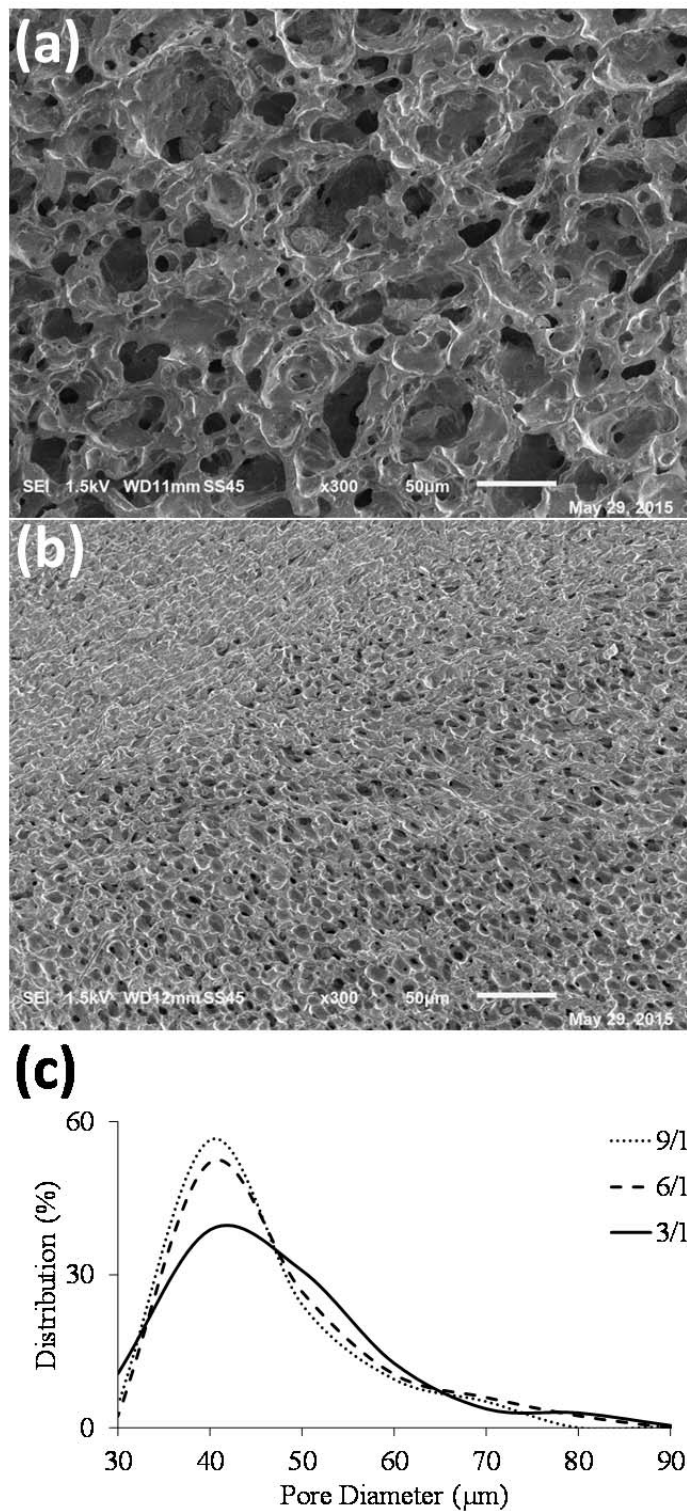
Figure 3-1. The SEM of 25% PU scaffolds with the NaCl/PU ratios of (a) 9/1 and (b) 0/1. (c) Distribution of 3D pore size with different NaCl/PU ratios derived by the Saltykov analysis.
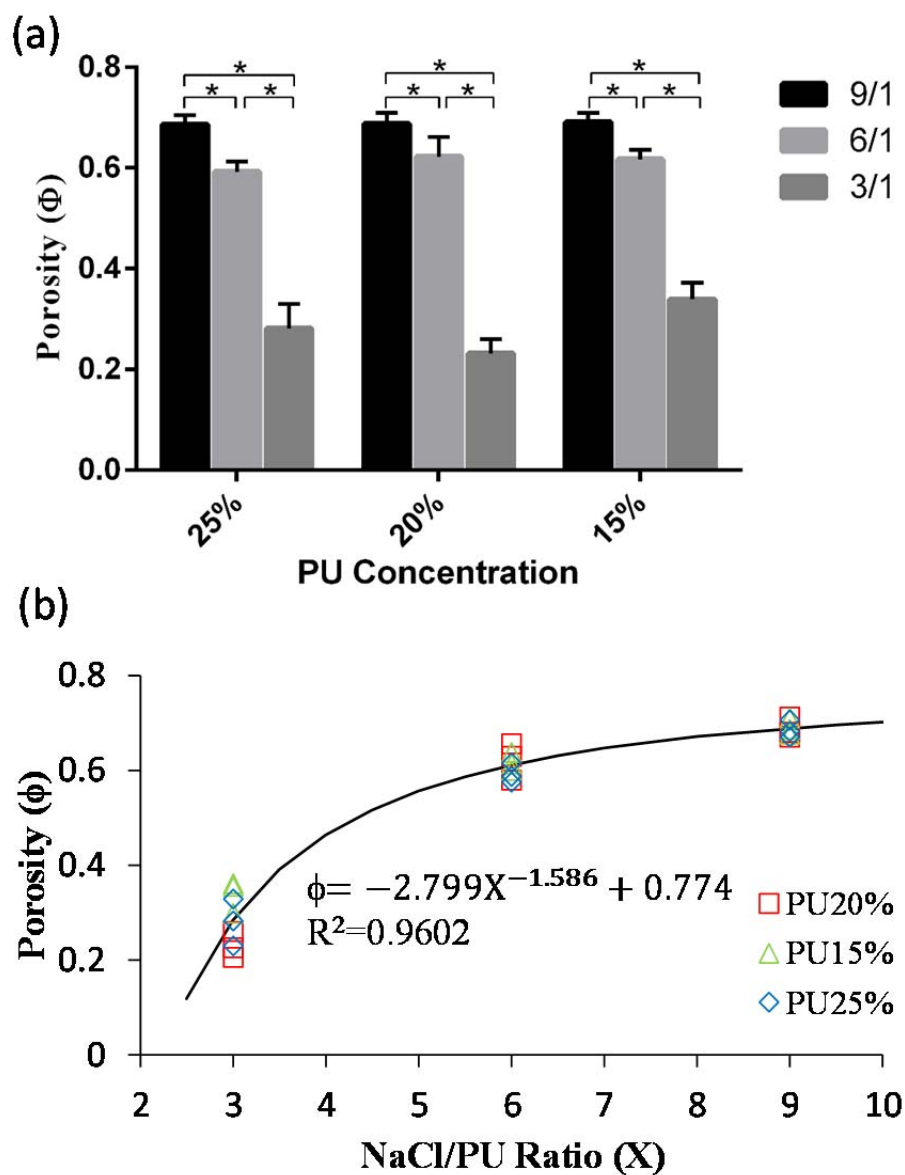
Figure 3-2. (a) The porosity of the PU scaffolds with different NaCl/PU weight ratios fabricated with three PU concentrations. (b) The relationship between NaCl/PU ratio and the porosity of the PU scaffolds (X ranged from 2.5 to 10). (* indicate p-values< 0.05)

Relationship between the porosity and mechanical properties of PU scaffolds

The mechanical strength of the PU scaffolds increased with increasing original PU concentration. The compressive (E_{Y0}^{-}) and tensile (E_{Y0}^{+}) moduli (MPa) of the PU scaffolds fabricated only by the phase inversion method can be described as a function of the original PU concentration (%) (Figure 3-3):

$$E_{Y0}^{+}=112C^{3.677}+1.089 \ (R^2=0.8) \tag{8}$$

$$E_{Y0}^{-}=1735 \ C^{5.778}+0.4352 \ (R^2=0.92) \tag{9}$$

where C is the PU concentration. The porosity of the PU scaffolds was significantly increased by the salt leaching method which dramatically reduced the mechanical strength of the PU scaffolds (Figure 3-4 a to c, 3-5 a to c). After normalized with the PU scaffolds fabricated by the phase inversion method only, changes in the compressive and tensile moduli of three different PU concentration groups were similar and depended on porosity only (Figure 3-4d and 3-5d). The relationship between the normalized tensile (E_Y^{+}) and compressive (E_Y^{-}) moduli and porosity can be expressed by the following functions:

$$E_Y^{+}=0.7698(1-\varphi)^{1.717} \ (R^2=0.91) \tag{10}$$

$$E_Y^{-}= 0.6291(1-\varphi)^{1.368} \ (R^2=0.88) \tag{11}$$
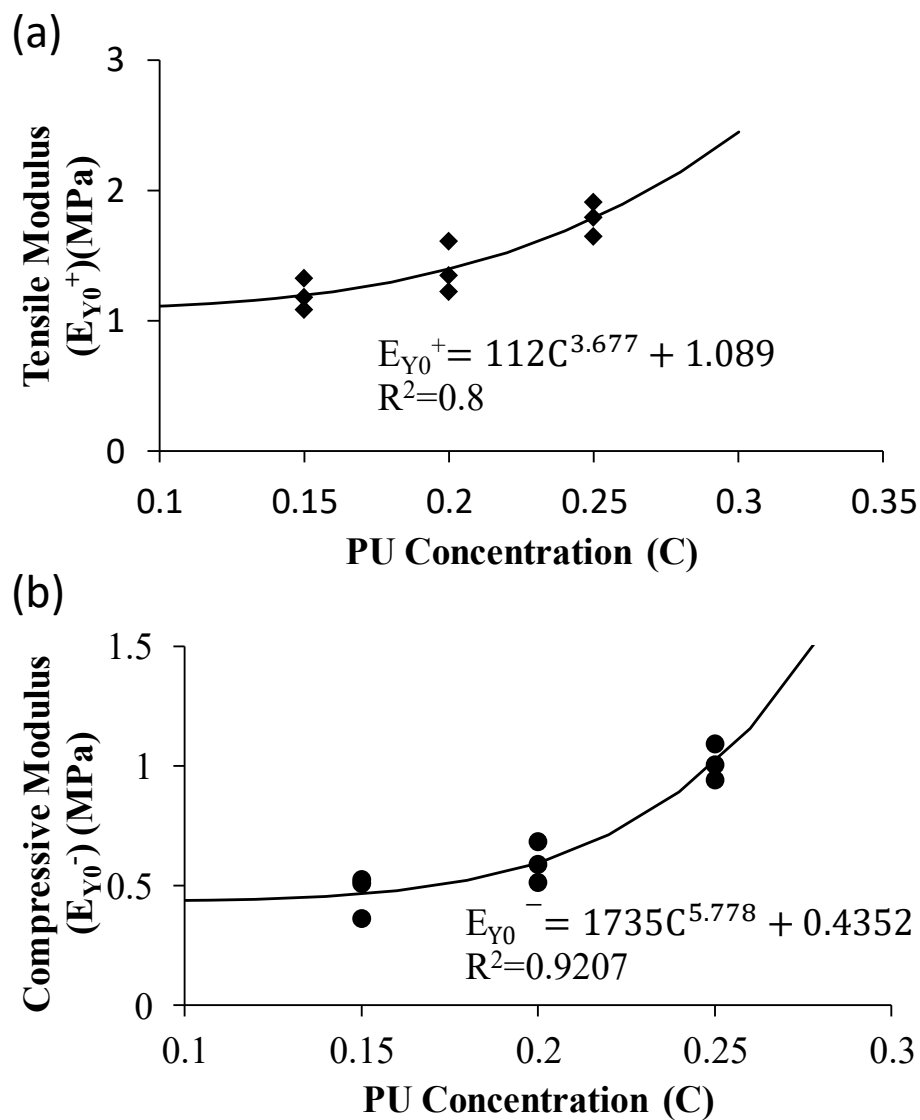
Figure 3-3. The relationships between the original PU concentration and the (a) ternsile and (b) compressive moduli of the PU scaffolds.
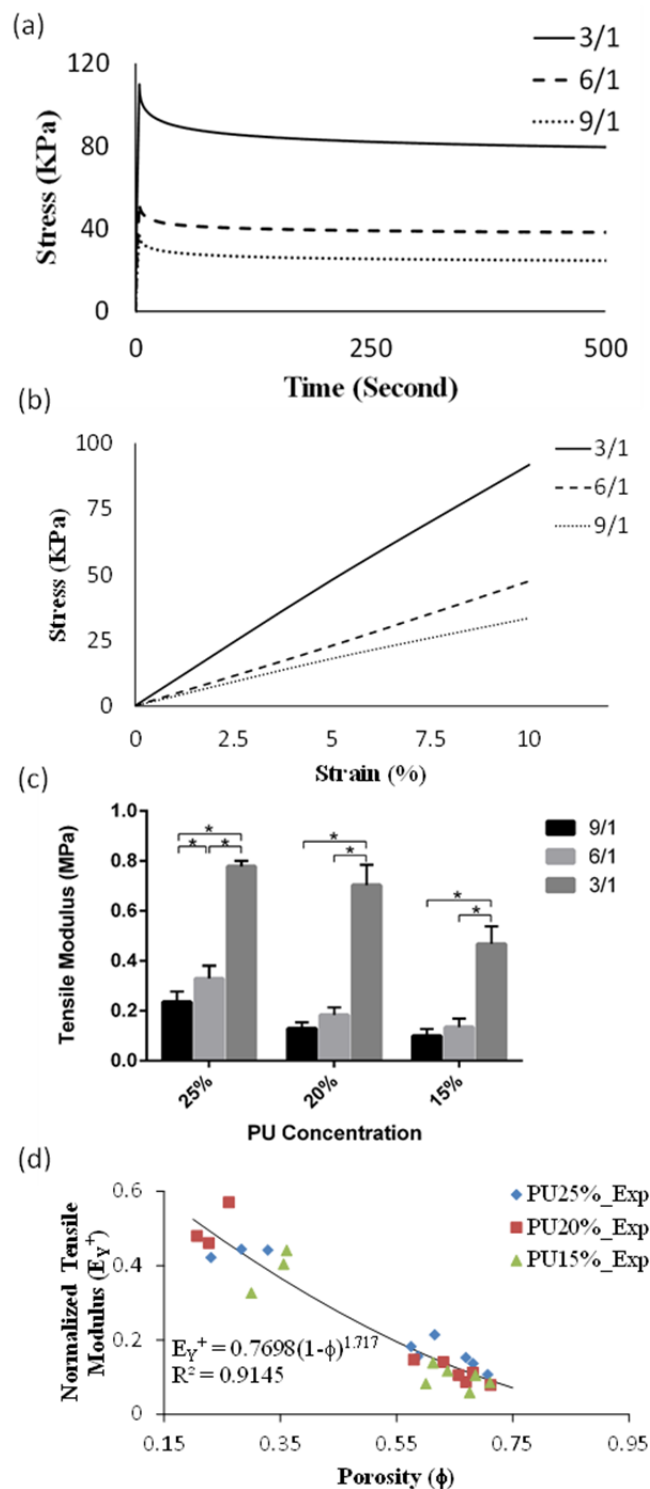
Figure 3-4. The typical (a) tensile stress relaxation curve and (b) linear elastic ramp of stress-strain curve of 25% PU scaffold with different NaCl/PU ratios. (c) The tensile modulus of the PU scaffolds with different NaCl/PU ratios. (d) The relationship between the porosity and normalized tensile modulus of the PU scaffolds. (* indicate p-values< 0.05)
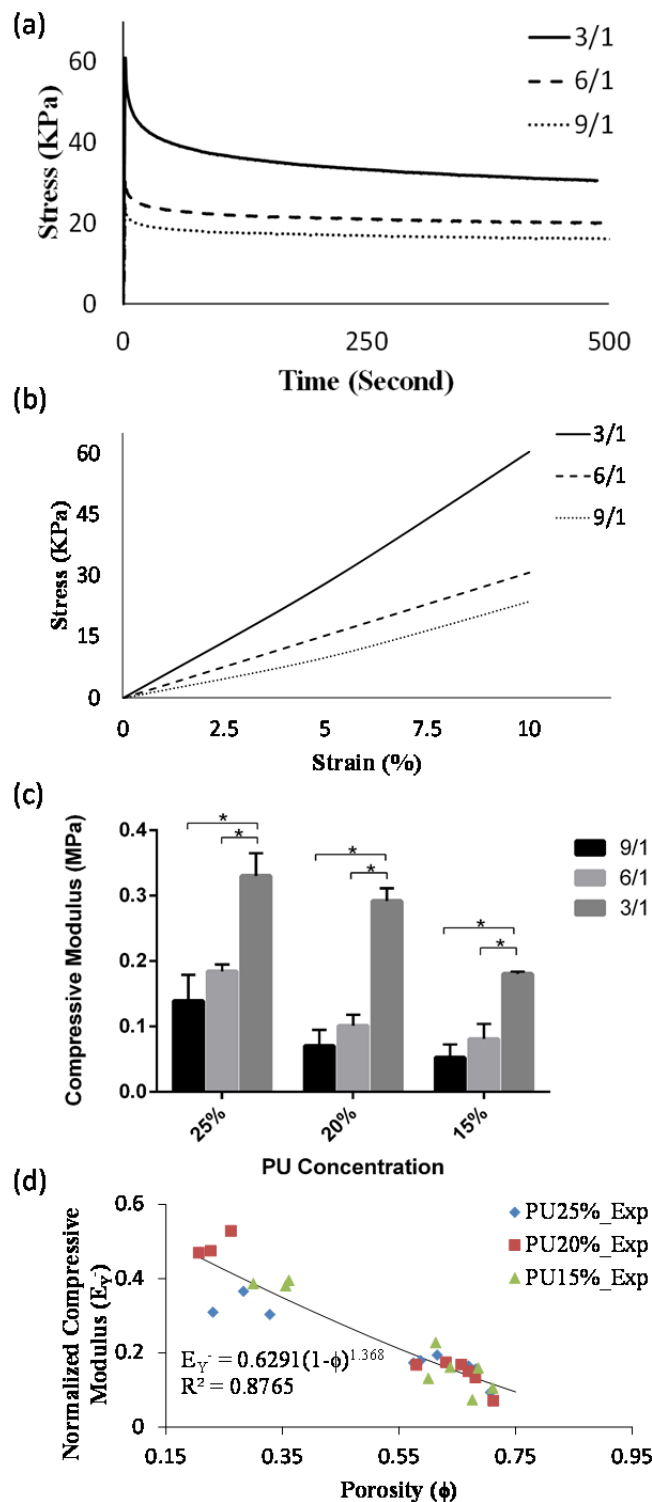
Figure 3-5. The typical (a) compressive stress relaxation curve and (b) linear elastic ramp of stress-strain curve of 25% PU scaffold with different NaCl/PU ratios. (c) The compressive modulus of the PU scaffolds with different NaCl/PU ratios. (d) The relationships between the porosity and normalized compressive modulus of the PU scaffolds. (* indicate p-values< 0.05)

Relationship between porosity and mass transport properties of PU scaffolds

Since the mass transport properties of porous scaffolds were determined by the features of pore structure which were found similarly for three different PU concentrations, only 25% PU was used to examine the relationship between porosity and mass transport properties of the PU scaffolds. The hydraulic permeability and glucose diffusivity of the PU scaffolds significantly increased with increasing porosity (Figure 3-6a and 3-7a). The permeability of the PU scaffolds was $2.86\pm0.95 \times 10^{-9}$ m^4/Ns, $3.49\pm2.39 \times 10^{-10}$ m^4/Ns and $9.41\pm3.12 \times 10^{-13}$ m^4/Ns for the NaCl/PU weight ratio of 9/1, 6/1 and 3/1, respectively. The relationship between the permeability (k) and porosity of the PU scaffolds can be described as (figure 3-6b):

$$ln(k)=ln(5.105 \times 10^{-11}(\varphi/1-\varphi)^{4.015}) \ (R^2=0.93) \tag{12}$$

The glucose diffusivity of the PU scaffolds was $5.01\pm0.84 \times 10^{-6}$ cm^2/s, $2.02\pm0.43 \times 10^{-6}$ cm^2/s and $2.65\pm0.76 \times 10^{-8}$ cm^2/s for the NaCl/PU weight ratio of 9/1, 6/1 and 3/1, respectively. The relationship between the glucose diffusivity and porosity of PU scaffolds can be described as (figure 3-7b):

$$ln(D/D_0)=-2.286 \ (1-\varphi/\varphi)^{0.9261} \ (R^2=0.91). \tag{13}$$

(a)

(b)

$$\ln(k)=\ln[5.105 \times 10^{-11}(\frac{\phi}{1-\phi})^{4.015}]$$
$$R^2=0.927$$
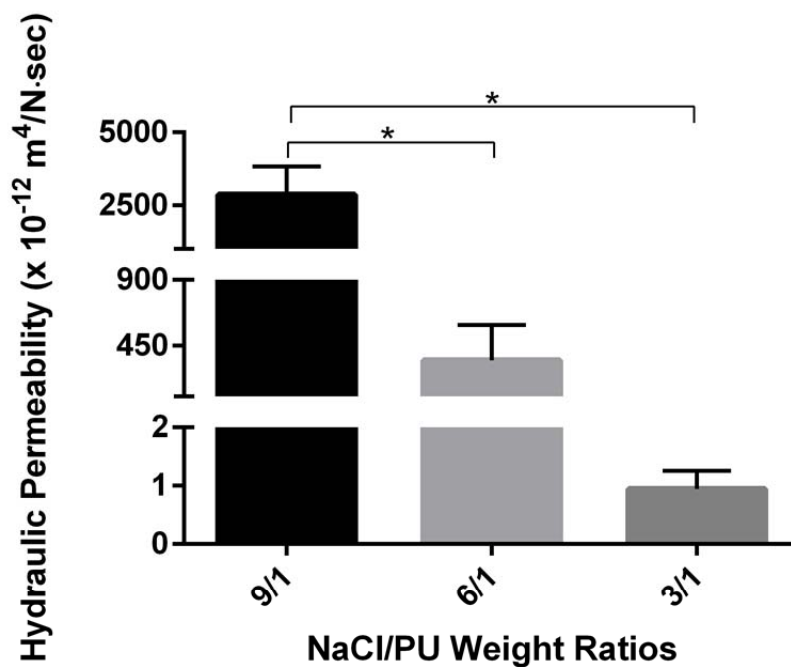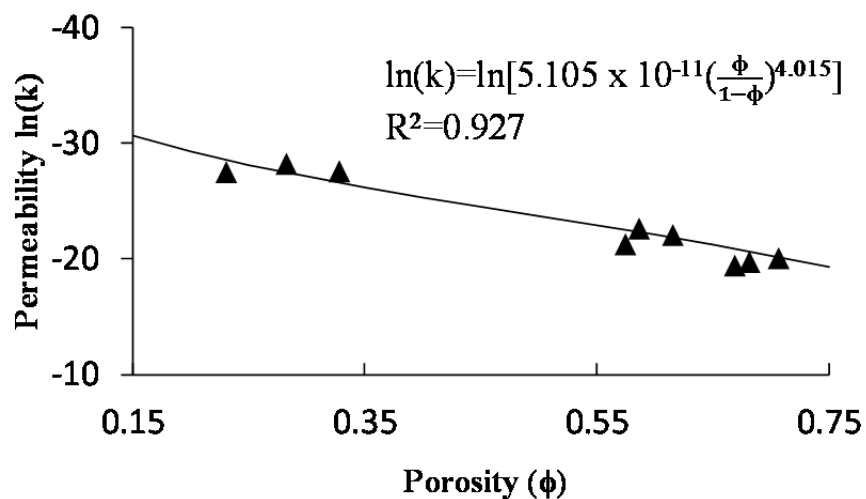
Figure 3-6. (a) The hydraulic permeability of the PU scaffolds with different NaCl/PU ratios fabricated using 25% PU. (b) The relationship between the porosity and hydraulic permeability of the PU scaffolds. (* indicate p-values< 0.05)
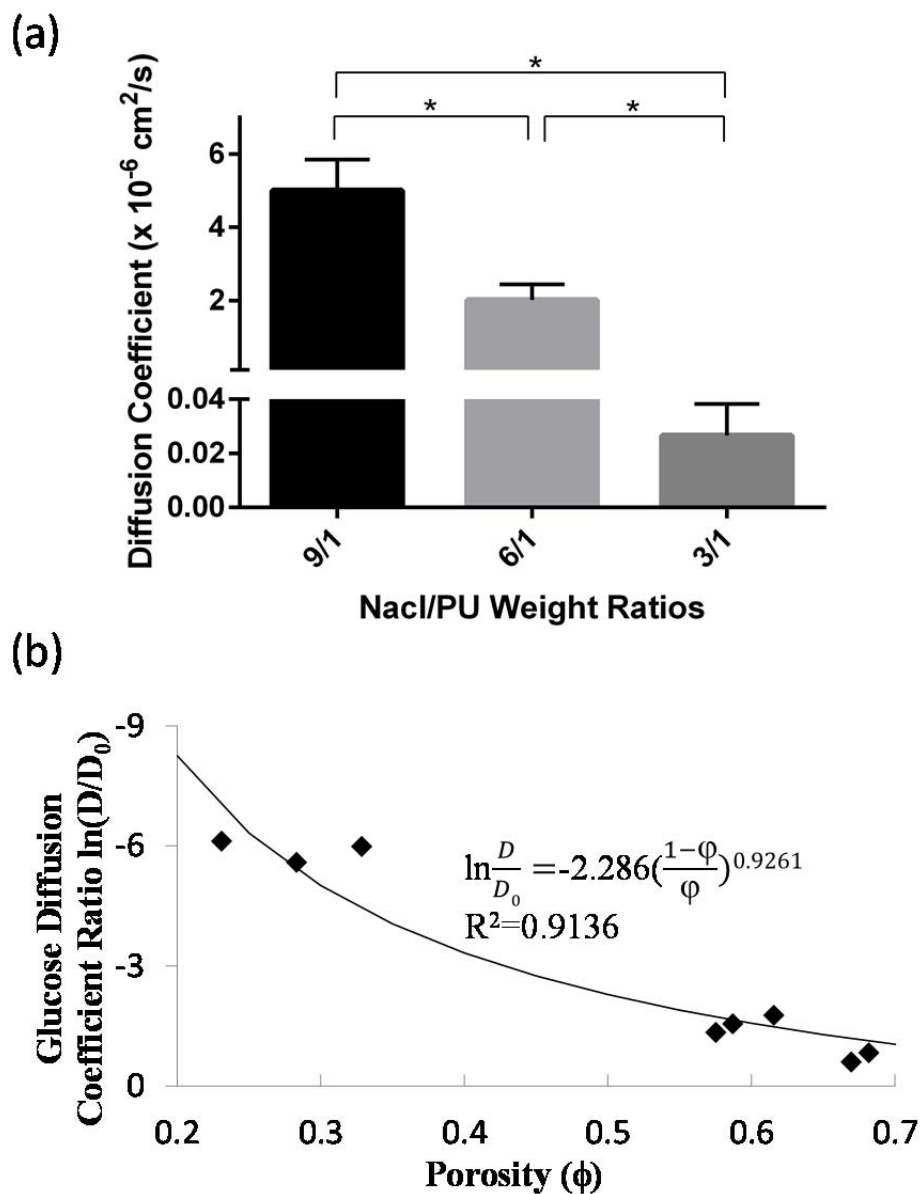
Figure 3-7. (a) The glucose diffusivity of the PU scaffolds with different NaCl/PU ratios fabricated using 25% PU. (b) The relationships between the porosity and glucose diffusivity of the PU scaffolds. (* indicate p-values< 0.05)

3.4 Discussion

This study systemically investigated the relationships between porosity and mass transport and mechanical properties of PU porous scaffolds. With similar pore sizes, the mass transport and mechanical properties of PU porous scaffolds can be described as single functions of porosity regardless of initial PU concentration. The results suggest that the porosity is a key parameter which governs both mass transport and mechanical properties of porous scaffolds. Since scaffold requirements are different in diverse tissue engineering applications, PU scaffolds with desired mass transport and mechanical properties can be fabricated by controlling their porosity. The methodology establishing of the relationships between porosity and mass transport and mechanical properties of porous PU scaffold can facilitate the design of specific scaffolds for tissue engineering.

The mass transport properties of porous scaffolds of tissue engineering are very important since nutrient delivery, waste removal, and protein transport are essential for the survival of cells seeded within scaffolds. Although the main mechanism of transport within porous scaffolds is diffusion, high permeability allows internal fluid flow to be induced by mechanical loading (e.g., compression and pressure gradient), prompting transport of molecules by convection. In addition, permeability modulates the magnitude of pressure and shear force (generated by fluid flow) which has been recognized as important mechanical factors for different applications of tissue engineering [111-115]. The mass transport properties (i.e., hydraulic permeability and molecular diffusivity) of porous scaffolds are mainly determined by the features of pore structure, such as porosity, interconnectivity and pore size and shape [116-118]. Previous studies also demonstrated the permeability of porous foams was reduced by compressive strain described as a

function of porosity [119, 120]. Permeability and diffusivity of biomaterials and biological tissues have been shown to be strongly associated with their porosity [92, 116, 121]. Hence, the porosity was one of the key factors that affected the mass transport properties of porous scaffolds. In this study, the relationship between porosity and mass transport properties of PU scaffolds can be described by single functions of porosity (i.e., Eqs. (4) and (6)). However, hydraulic permeability was found to be more sensitive to changes in porosity than glucose diffusivity. In this study, when the averaged porosity of PU scaffolds increased from 28 % (NaCl/PU ratio of 3/1) to 68% (NaCl/PU ratio of 9/1) (2.5-fold increase), the permeability and glucose diffusivity exhibited 3000- and 190-fold increases, respectively. This finding is consistent with previous agarose studies [107, 110]. Previous studies have demonstrated dynamic loading can promote solute transport in porous media [122, 123]. Dynamic loading may be a potential strategy to promote nutrient transport in PU scaffolds with low porosity. However, since the influence of dynamic loading on solute transport in porous media depends on the size of solutes (i.e., diffusivity) and permeability, further studies are needed to examine the effects of dynamic loading on solute transport in PU scaffolds with different combinations of diffusivity and permeability. Furthermore, since glucose is the main nutrient for production of intracellular energy, which is essential for cellular activities, glucose diffusivity was determined in this study. Diffusivities of different molecules mainly depend on their sizes in the same medium [110]. Therefore, diffusivities of other molecules in PU scaffolds could be estimated from glucose diffusivity determined in this study based on the ratio of molecular sizes [110].

Incorporating salts into PU scaffold creates larger pores which cause the disruption

of the continuity in the scaffold structure. The large pores act as weak points in the scaffold, which make the structure brittle and easily to break down under loading [81]. Thus, high porosity weakens the mechanical strength of porous scaffolds. This study showed that when the porosity increased from about 25% up to 70%, the normalized tensile and compressive modulus decreased about 5 times (from about 0.5 to 0.1). This finding is supported by previous studies [79, 87, 89]. Furthermore, it is well known that the mechanical properties of the biological tissues and biomaterials are strongly associated with their apparent density by a power law relation [95, 98, 124]. Since the apparent density of porous materials is a function of porosity, a power law has been used to relate the mechanical strength of porous scaffolds with their porosity [95-98]. Jones, et al. performed a theoretical simulation on the mechanical properties of hydroxyapatite scaffolds with on different porosities and found a power law trend between the porosity and reduced Young's modulus of hydroxyapatite scaffolds [95, 96]. In this study, the tensile and compressive moduli of PU scaffolds were increased with increasing PU concentration. However, the relationship between the porosity and normalized mechanical properties of PU scaffolds can be described by a power law (i.e., Eq. (2)), independent of initial PU concentration.

The salt leaching process is one of the most common and relative easiest methods to fabricate a porous scaffold structure [81]. In this study, the porosity of PU scaffolds depends on the salt-polymer weight ratio used in the salt leaching method, while the size of the pores generated was determined by the size of salt crystals incorporated. Although the relationships between porosity and scaffold properties were investigated in this study, the influence of pore size on scaffold properties was not examined. The relationships

developed in this study was specific for the PU scaffolds with pore size around 40 μm. Pore size has been shown to affect the mechanical properties of porous scaffolds with the same porosity [125, 126]. O'Brien, et al. also demonstrated that the permeability of collagen scaffolds increased with increasing pore size [120]. Moreover, molecular diffusivity in porous scaffolds depends on their permeability which is determined by porosity and pore size [117, 127]. This study demonstrated that with the same pore size, a particular set of diffusivity and permeability of PU scaffolds can be determined by a specific porosity. Similarly, with the same porosity, different pore sizes may result in different magnitudes of diffusivity and permeability of scaffolds [94, 116, 117]. In addition to pore size, the other limitation of this study is the limited range of porosity. The porosity of our PU scaffolds falls into the range 30% to 70%. The PU sample with the minimum porosity (11.39±3.01%) can be fabricated without incorporation of NaCl. Although the porosity increases with increasing salt-polymer ratio, it may reach a plateau around 80% based on our results (Figure 3-2b). Therefore, the maximum porosity may be achieved only at the level 80% by the current fabrication protocol. Nevertheless, since pore size and porosity created by the salt leaching process can be easily controlled by salt size and salt-polymer ratio. A unique combination of mass transport and mechanical properties of PU scaffolds may be created by controlling a specific pore size and porosity using the salt leaching method.

The relationships between scaffold porosity and properties described in this study can be utilized for fabrication of PU porous scaffolds with specific mechanical and mass transport properties (Figure 3-8). For instance, to fabricate a porous PU scaffold with a specific glucose diffusivity (D*) or permeability (k*) and a specific compressive or

tensile Young's modulus (E_Y^*), a porosity (φ^*) can be determined using either Eq. (12) or (13) based on D^* or k^*, and then used to determine a normalized Young's modulus (E'_Y) using Eq. (10) or (11). Based on the normalized modulus (E'_Y), the Young's modulus (E_{Y0}) of original PU scaffold (fabricated with the phase inversion method only) can be calculated (i.e., $E_{Y0} = E_Y^* / E'_Y$). An initial PU concentration can be determined by Eq. (8) or (9) based on E_{Y0}, while a salt/ PU ratio can be determined using Eq. (7) based on φ^*. Finally, the porous PU scaffold with E_Y^* and D^* or E_Y^* and k^* can be fabricated using the salt leaching method with the initial PU concentration and salt/ PU ratio determined.

3.5 Conclusion

In summary, this study systemically investigated the relationships between porosity and mass transport and mechanical properties of PU porous scaffolds. With similar pore sizes, mass transport properties can be described by single functions of porosity. In addition, the relationships between normalized mechanical properties and porosity can also be described by power law functions regardless of initial PU concentration. By using the relationships between scaffold porosity and properties, porous PU scaffold with desired mass transport and mechanical properties could be fabricated by controlling scaffold porosity for different tissue engineering applications. The systematic approach established in this study can be also applied to characterization of other biomaterials for facilitating scaffold design and fabrication.

```
┌─────────────────────────────────┐
│ To fabricate PU scaffolds with  │
│ desired Young's modulus (E_Y*)   │
│ and glucose diffusivity (D*) or  │
│ permeability (k*)               │
└─────────────────────────────────┘
                 │
                 ▼
┌─────────────────────────────────┐
│ Based on D*or k*, a porosity φ * │
│ is determined based on Eq. (12) │
│ or (13)                         │
└─────────────────────────────────┘
       │                     │
       ▼                     ▼
┌──────────────────┐  ┌──────────────────┐
│ Based on φ*, a    │  │ Based on φ*,      │
│ specific          │  │ normalized modulus │
│ NaCl/PU ratio is  │  │ E'_Y is determined │
│ determined based on│  │ based Eq. (10) or (11) │
│ Eq. (7)           │  └──────────────────┘
└──────────────────┘           │
       │                       ▼
       │            ┌──────────────────────┐
       │            │ The pure PU Young's   │
       │            │ modulus E_{Y0} = E_Y*/E'_Y │
       │            │ is calculated and used │
       │            │ to determine initial   │
       │            │ pure PU concentration  │
       │            │ with Eq. (8) or (9)    │
       │            └──────────────────────┘
       │                       │
       ▼                       ▼
┌─────────────────────────────────────────┐
│ Porous PU scaffold with E_Y* and D* or E_Y* and │
│ k* can be fabricated using the salt leaching │
│ method with the initial PU concentration and │
│ NaCl/PU ratio determined.                │
└─────────────────────────────────────────┘
```

Figure 3-8. The flow chart of fabricating PU porous scaffolds with specific mechanical and mass transport properties

Chapter 4: Enhancement of Energy Production of the Intervertebral Disc by the Implantation of Polyurethane Mass Transfer Devices

4.1 Introductory Remarks

As mentioned in previous chapters, the IVD is the largest avascular tissue in human body, and insufficient nutrient supply has been suggested to be one of the etiologies for disc degeneration [5, 6]. The exchange of nutrients and metabolites in the IVD are mainly driven by concentration gradients [13]. This results in the central region of the IVD having lower levels of oxygen, glucose and other nutrients compared to the outer region [14, 15]. As long as the nutrient level remains above a vital threshold, the viability and functionality of the IVD can be maintained. When nutrient demand exceeds supply, it results in decreased cell activity level and may ultimately cause cell death [17, 18]. It is observed that calcification of the vertebral endplate with age causes a reduction in the nutrient level in the NP region [19-21]. This loss of nutrients is detrimental to cellular functions such as ECM production and may ultimately result in disc degeneration. Addressing and supplementing nutrient supply could be one of the potential treatment strategies for treating or reversing disc degeneration.

Most of the cell activities in the IVD such as ECM production and maintenance are high energy demanding processes which require ATP as fuel [22]. ATP also plays an important role for biosynthesis of PGs [23, 24] which are one of the major ECM components in the IVD. Additionally, ATP is an extracellular signaling molecule that mediates a variety of cellular activities through purinergic signal pathways [25-27]. Our previous study demonstrated that mechanical loading promotes ATP production and release from IVD cells [28] while extracellular ATP can modulate the ECM biosynthesis

43

of IVD cells [29]. Since ATP is one of the key factors in maintaining the integrity and function of the IVD, chronic malnourishment and loss of ATP concentration may lead to cell death and ultimately IVD degeneration.

Recent studies have shown that several biomaterials implanted for closure of AF defects maintain the height and stability of the IVD [34-36]. Since there are ample nutrient supplies at the edges of AF due to blood supply, porous materials with high transport properties implanted in AF can be designed to facilitate transport of nutrients from the edge of AF into the NP region in order to promote cellular energy production. In addition, the importance of matching AF mechanical properties has been emphasized on developing successful biomaterials for AF repair [128]. Our previous study has systematically characterized the relationships between the transport and mechanical properties of PU porous scaffolds and demonstrated that the PU porous scaffolds can exhibit higher transport properties and similar mechanical strength compared to AF tissues [129]. Therefore, the objective of this study was to investigate the enhancement of ATP production in the IVD by the implantation of porous PU scaffolds in the AF as a passive mass transfer device.

4.2 Materials and Methods

Fabrication of PU mass transfer devices

The PU mass transfer device was fabricated by a salt leaching/phase inversion method based on our previous studies [80, 129]. The procedure is as follows: a PU solution of 25% (w/v) was prepared by dissolving PU pellets (Tecflex® SG-85A, Lubrizol, Wickliffe, OH) in N,N-dimethyl formamide (DMF; Sigma-Aldrich, St. Louis,

Mo). Sodium chloride (NaCl; Sigma-Aldrich) crystals were ground and sieved to select sizes smaller than 70 μm and were mixed with the PU solution at 9/1 (NaCl/PU) weight ratios. Polytetrahydrofuran (Sigma-Aldrich) was also added to the NaCl-PU mixture in 25% (v/v) volume ratio as a soluble filler to enhance the interconnectivity of the porous scaffolds. The mixed solution was well stirred and then injected into glass cylinder molds. Porous PU scaffolds were formed by submerging the cylinder molds in 65% of ethanol with 1% DMF via phase inversion for 48 hours. After separating from the molds, the porous PU scaffolds were rinsed in distilled water for 24 hours in order to remove NaCl crystals. After the rinsing step, the porous PU scaffolds (diameter: 2.5 mm, long: 25 mm) were preserved in PBS and utilized as mass transfer devices for the further experiments. The device length of 25 mm was chosen because of sufficient length (8 mm) in NP region and better manipulation during the insertion procedure.

Mass transfer device experiment

The lumbar spines were obtained from Yorkshire pigs of both sexes (age: 14~16 weeks; weight: 80~100 lbs.) within 2 hours of sacrifice (Department of Veterinary Resource, Miami, FL). Three FSUs (L2 to L5) were isolated from each pig by making transverse cuts through the vertebrae by a sterile bone saw. The sectioned planes of vertebrae were sealed with bone cement (P.A.R. Brand Acrylic Resin, Wheeling, IL) in order to block nutrient diffusion pathway through endplate route and to simulate endplate calcification conditions.　After washing with PBS containing 10% of antibiotic-antimycotic (Lonza, Walkersville, MD) and 100 μg/ml of gentamicin sulfate (Lonza) for 3 times, the FSUs from each pig were randomly divided into 3 experimental groups:

intact, device, and surgical groups. For the device and surgical groups, two puncture holes (diameter smaller than 2.5 mm) were created bilaterally using sterile needles at the dorsal side of the AF region without removing tissue. The PU mass transfer devices were squeezed and implanted under a press-fit condition in the device group only (Figure 4-1a). All of the experimental groups were cultured in low glucose (1g/L) Dulbecco's Modified Eagle Medium (DMEM, Invitrogen, Carlsbad, CA) containing 1% of antibiotic-antimycotic and 50 µg/ml of gentamicin sulfate at 37°C, 5% CO_2, and 20% O_2 within an incubator. After 7 days of culture, a transverse cut was made at the mid-disc height of the FSUs to expose the NP and AF regions. Tissue samples (~25mg) were harvested from three different locations (AF, peripheral NP and central NP regions) along PU mass transfer devices in the device group and the same locations in the intact group (Figure 4-1b). Additionally, the sealing effect of PU mass transfer devices was examined before and after 7 days of culture. The FSUs with implantation of PU transfer device were incubated in the PBS containing 1 mg/ml Fluorescein (Sigma-Aldrich) for 36 hours. A transverse cut was made at mid height of the FSU and fluorescence images were captured using the BioSpectrum imaging system (UVP, Upland, CA).

(a)

(b)
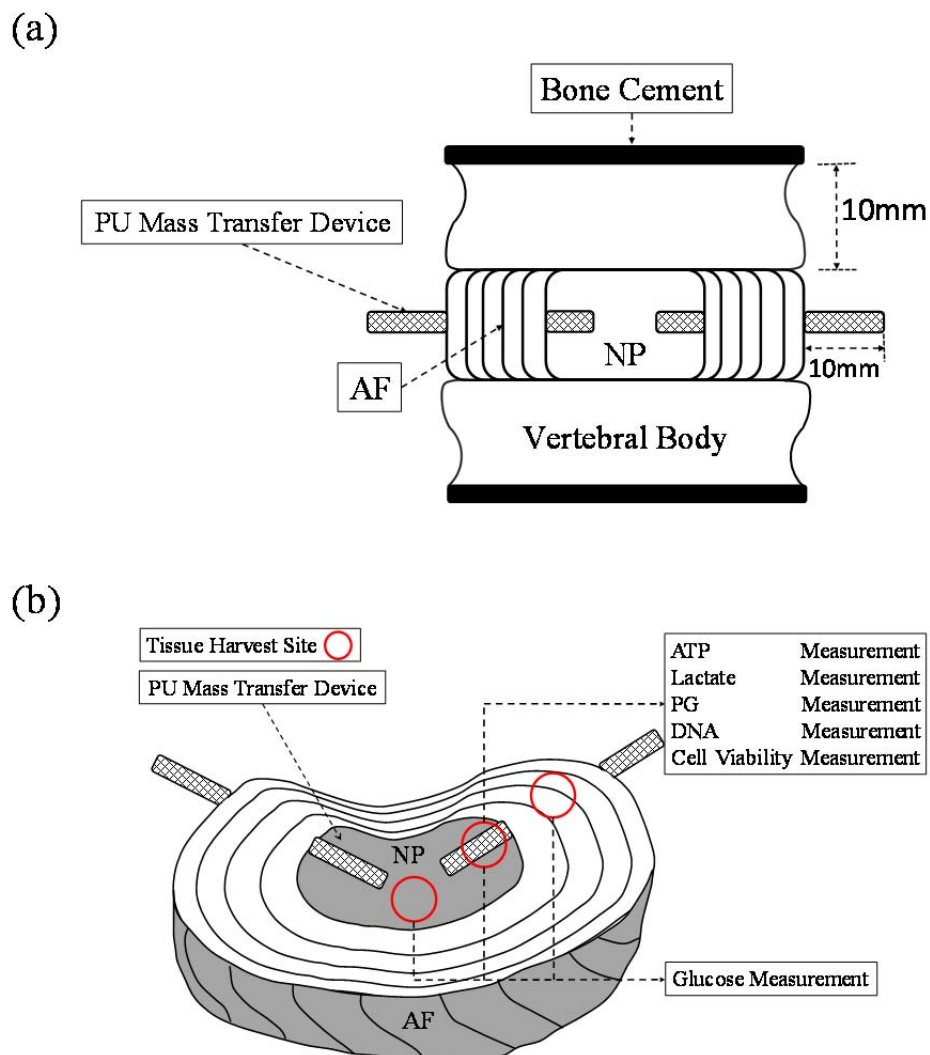
Figure 4-1. (a) Schematic of FSU preparation with PU mass transfer device. (b) Locations of PU mass transfer devices implantation and tissue harvest sites including central NP, peripheral NP and AF regions.

Disc height measurement

The disc height of each group (n=11) was measured from endplate to endplate at 3 different random locations by a digital caliper (Mitutoyo 500-196-20, Aurora, IL, accuracy ± 0.025 mm) before and after 7 days of culture.

Mechanical testing

Uniaxial compressive tests were performed to determine the compressive structural stiffness of the IVD before and after 7 days of culture based on the protocol described previously [35]. A custom-made loading system developed in our laboratory [28] was used for the compressive tests. The FSUs from each group (n=8) were first applied with a compressive preload of 0.5 kg, followed by a dynamic compressive strain of 5% with a frequency of 0.1 Hz. The 25th loading cycle was used to determine the compressive stiffness which was calculated by a linear regression of the load-displacement curve between 60% and 100% of the maximal load [35].

Glucose measurement

The tissue samples harvested from the intact and device groups were analyzed for glucose concentration (n=8). Tissue samples (~25 mg) were boiled for 5 minutes with 500 µl of 3 mM EDTA (Sigma-Aldrich). After addition of 500 µl PBS solution containing 250 µg/ml of papain (Sigma-Aldrich) and 10 mM of EDTA, the samples were incubated in the heater at 65°C for 16 hours [130]. Next, the glucose concentration was measured by the glucose (GO) assay kit (Sigma-Aldrich). The tissue digestion solutions of 50 µl were first mixed with 100 µl of the assay reagent and incubated at 37 °C for 30

mins. After the incubation, 100 µl of sulfuric acid (VWR, Radnor, PA) was added and the absorbance was measured at 540 nm by a multimode detector (DTX880, Beckman Coulter, Brea, CA). Tissue density was measured using a density determination kit and an analytical balance (Sartorius, Germany) for calculation of tissue volume [131]. Glucose concentration was calculated by dividing the glucose content by tissue volume.

Cell viability

The tissue samples (n=5) from peripheral NP location in the intact and device groups were analyzed for cell viability. The Hoechst 33258 dye (Polysciences, Warrington, PA.) was used to identify the total number of cells and ethidium homodimer-1 (Biotium, Fremont, CA) was used for dead cell staining [132]. The images were analyzed by ImageJ software for cell counting.

ATP measurement

A modified phenol extraction method combining the luciferin-luciferase assay (Sigma-Aldrich) were utilized for ATP measurement (n=13) [133]. Tissue samples (~25 mg) from peripheral NP location in the intact and device groups were first homogenized with 500 µl of water saturated phenol (Sigma-Aldrich), and then mixed with 500 µl of chloroform (Sigma-Aldrich) and 300 µl of de-ionized water. The mixed solution was thoroughly shaken for 20 secs and centrifuged at 13000 rpm for 10 min at 4 °C. The supernatants were diluted 1000-fold with de-ionized water and mixed with the assay reagent with 1 to 9 volume ratio and the luminescence was measured immediately by the multimode detector.

Lactate measurement

Lactate measurement was based on the protocol described in our previous study (n=13) [134]. A lactate reaction reagent was made by dissolving 5 mg/mL of β-nicotineamide adenine dinucleotide (Sigma-Aldrich), 0.2 M glycine buffer (Sigma-Aldrich) and 22.25 units/mL of L-lactic dehydrogenase (Sigma-Aldrich) in de-ionized water. Tissue samples (~25 mg) from peripheral NP location in the intact and device groups were digested with papain as described in the section of glucose measurement. The tissue digestion solutions were mixed with the lactate reaction reagent with 1 to 1 volume ratio, and the absorbance of 340 nm was measured by the multimode detector.

PG measurement

PG content was quantified by using the dimethylmethylene blue (DMMB) dye-binding assay which was described in our previous study (n=13) [29]. Tissue samples (~25 mg) from peripheral NP location in the intact and device groups were digested with papain as described in the section of glucose measurement. The tissue digestion solutions were diluted 11-fold with de-ionized water and mixed with DMMB dye solution with 1 to 20 volume ratio, and the absorbance of 525 nm was measured by the multimode microplate reader (SpectraMAx M2, Molecular Device, Sunnyvale, CA). The PG content was normalized by tissue weight.

DNA measurement

The extraction and digestion solutions for ATP and lactate measurements were also examined for DNA content (n=13). The Hoechst 33258 fluorometric assay was used for

the DNA content measurement [130]. In brief, 20 µl of sample solution was first mixed with 200 µl of working solution which contained 0.15 µg/ml of Hoechst dye, 100 mM Tris (Bio-Rad, Hercules, CA), 1 mM EDTA and 0.2 M NaCl. The DNA content was measured by the multimode microplate reader with excitation at 365 nm and emission at 458 nm.

Statistical analysis

A one-way ANOVA followed by a Bonferroni post-hoc test was performed to analyze differences in compressive stiffness reduction and disc height changes among three experimental groups. A paired t-test was also performed to analyze differences in disc height changes of each experimental group before and after 7 days of culture. For glucose concentration, a one-way ANOVA followed by a Bonferroni post-hoc test was also performed to analyze the differences among harvest locations. The ATP and lactate contents were normalized by the DNA content, and then each of device groups was normalized by its respective intact group. The student's t-test was performed to analyze differences in glucose concentration, cell viability, and ATP, lactate, PG and DNA contents between the intact and device group. The statistical analyses were performed using SPSS software (IBM, Chicago, IL). A $p < 0.05$ was considered statistically significant.

4.3 Results

Tissue-device sealing condition

After 7 days of culture, the length of PU mass transfer device outside the AF region remained 10 mm and no extrusion was observed (Figure 4-2a). In the sealing test, the results from day 0 and 7 showed that fluorescent solution diffused into the disc via the PU mass transfer device and there was no leaking at the boundary between the device and AF region after 36 hours of incubation (Figure 4-2b). The puncture holes in device group were still tightly sealed by the PU mass transfer devices.

Disc height

A significant increase in disc height was seen in the intact and device groups (9.04 ± 7.64 % and 5.63 ± 5.78 %, respectively) whereas disc height significantly decreased in the surgical group (-2.99 ± 4.06 %) (intact and device: $p < 0.01$; surgical: $p = 0.032$). When comparing disc height change among three experimental groups, the surgical group was significantly ($p < 0.01$) different from other two groups whereas no statistical difference was found between the intact and device groups (Figure 4-3e).

Compressive stiffness

Generally, the compressive stiffness was reduced for three experimental groups after 7 days of culture (Figure 4-3 and Table 4-1). When comparing among three groups, a significant reduction was found in surgical group (47.8 ± 14.8 %) (surgical-intact: $p = 0.012$; surgical-device: $p = 0.019$). In addition, there was no statistical difference between the intact and device groups. (29.7 ± 9.5 % and 30.8 ± 8.2 %, respectively) (Figure 4-3 a to d)

(a)

(b)
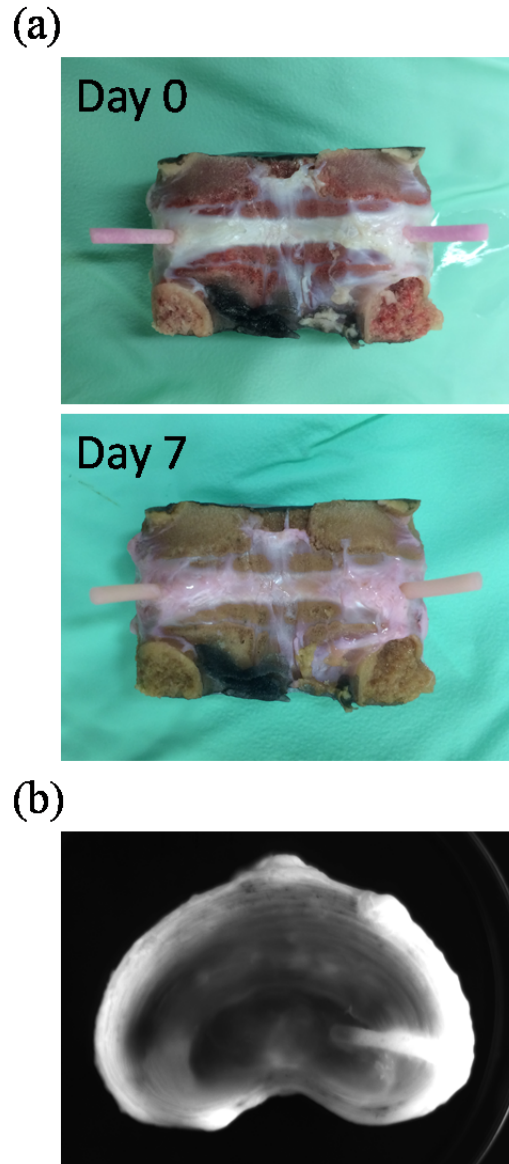
Figure 4-2. (a) The typical image of tissue-device boundary at day 0 and day 7. (b) The typical fluorescence image of the mid-height cross section of the IVD from day 0 after 36 hours of incubation with PBS containing Fluorescein.
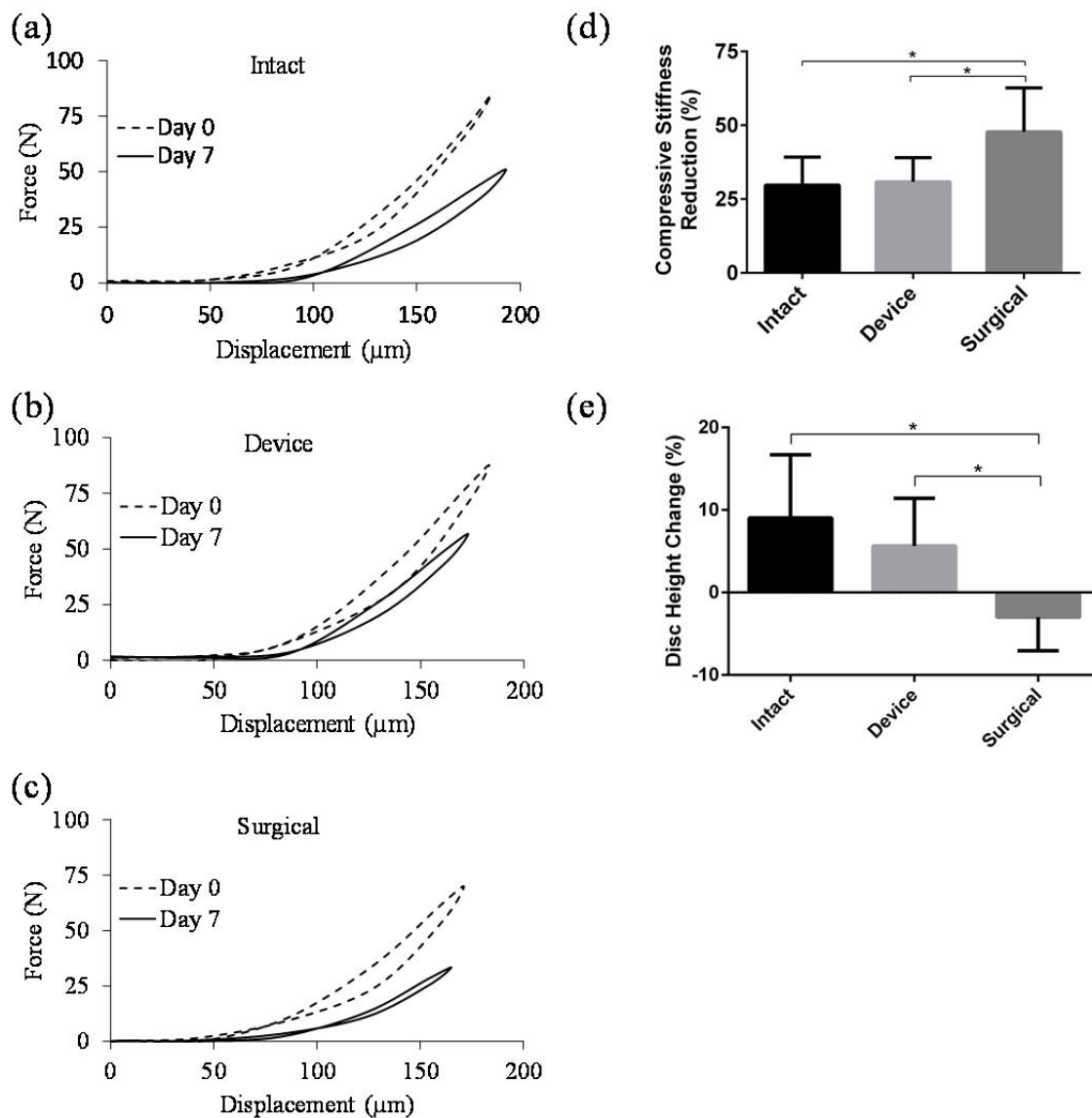
Figure 4-3. The typical force-displacement curves from the compressive tests of (a) intact, (b) device and (c) surgical groups. Comparison of (d) compressive stiffness reduction and (e) disc height change among the experimental groups. (* indicate p-value <0.05)

Table 4-1. The compressive stiffness of the porcine IVD from the intact, device and surgical groups at day 0 and 7.

Compressive Stiffness (N/mm)		
	Day 0	**Day 7**
Intact	1406.2 ± 555.1	959.8 ± 315.4
Device	1440.6 ± 500.4	977.6 ± 343
Surgical	1292.4 ± 518.1	650.9 ± 236.6

Glucose concentration

The glucose concentration at central NP, peripheral NP and AF region was showed in figure 4-4. A gradually decreasing of glucose concentration from AF to central NP region was found in both experiment groups. There was no statistical difference between intact and device groups at three harvest locations after 7 days of culture. However, a slight increase of glucose concentration was exhibited at NP region in device group.

Cell viability and DNA content

No significant differences were found in cell viability staining between the intact and device groups (90.14 ± 2.73 % and 89.16 ± 2.22 %, respectively) with both groups showing high cell viability after 7 days of culture (Figure 4-5). Similar DNA contents were found in tissue samples using the phenol and papain extraction methods. No statistical differences were seen in DNA content between the intact and device groups (phenol: 1 ± 0.42 and 0.98 ±0.44; papain: 1 ± 0.42 and 0.97 ± 0.45, respectively).

ATP, lactate and PG contents

With PU mass transfer device implanted for 7 days, the ATP content in the NP region was significantly higher in the device group than the intact group (intact: 1 ± 0.55; device: 2.71 ± 1.83) ($p < 0.01$) (Figure 4-6a). Similarly, the device group exhibited significantly higher lactate (intact: 1 ± 0.46; device: 1.93 ± 0.92) and PG contents (intact: 33.41 ± 5.73 µg/mg; device: 37.69 ±2.3 µg/mg) in the NP region than the intact group (lactate: $p < 0.01$; PG: $p = 0.024$) (Figure 4-6b and 4-6c).
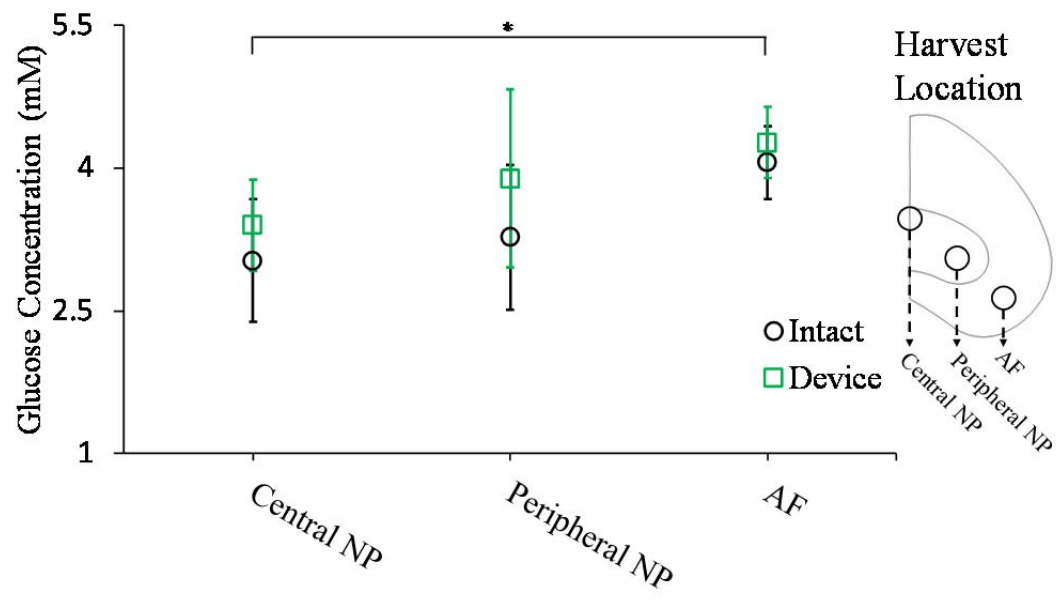
Figure 4-4. Comparison of the glucose concentration at central NP, peripheral NP and the AF regions between the intact and device groups. (* indicate p-value <0.05)
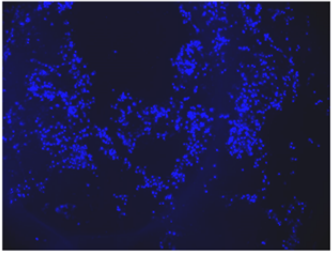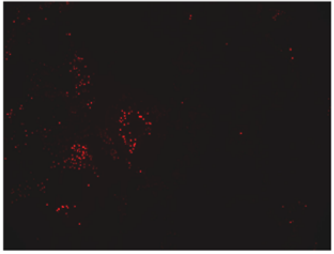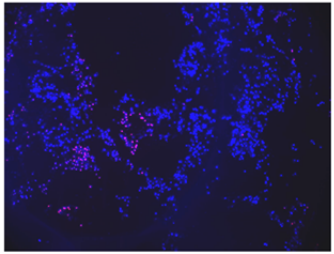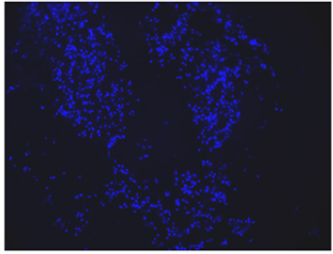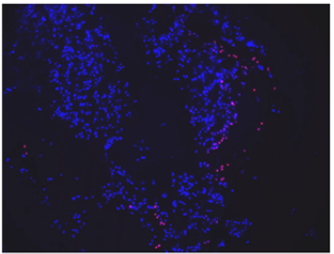
Figure 4-5. The typical cell staining of the intact and device groups.
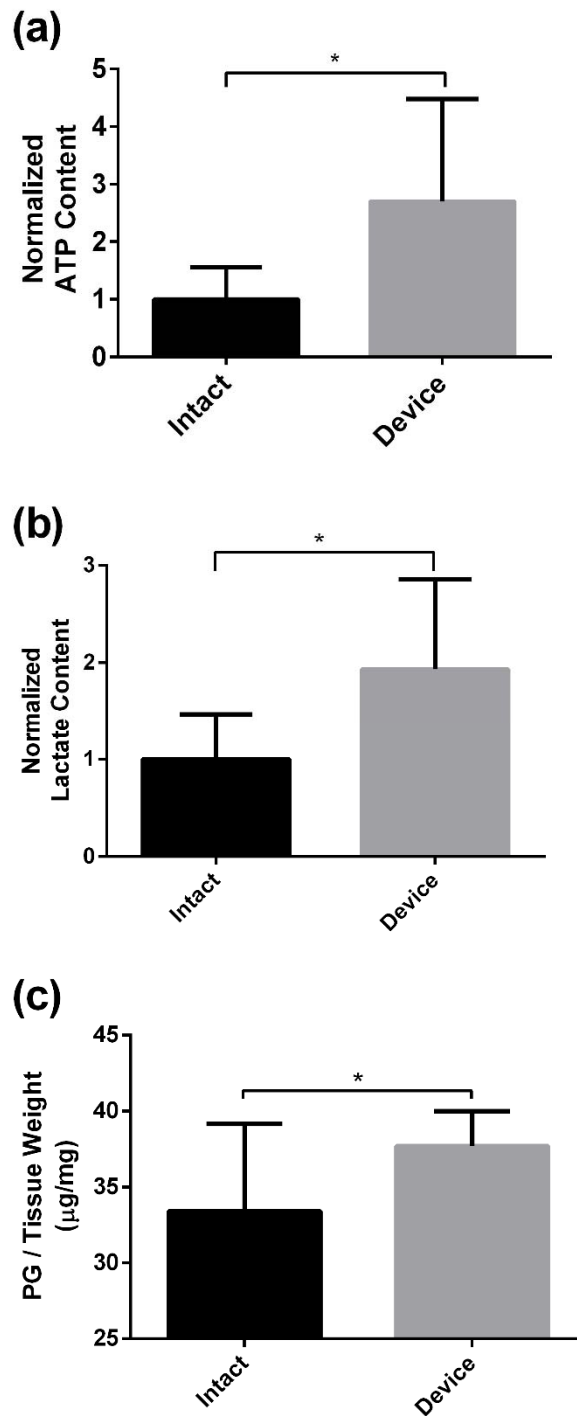
Figure 4-6. Comparison of the (a) ATP, (b) lactate and (c) PG contents between the intact and device groups. (* indicate p-value <0.05)

4.4 Discussion

This study investigated the effect of PU mass transfer device implantation on the metabolism of ATP and ECM in the porcine IVD after 7 days of culture. It was found that implantation of PU mass transfer devices increased the production of ATP and PG in the IVD while avoiding negative effects of the PU mass transfer devices on the structural stiffness and height of the IVD. This is the first study to demonstrate the feasibility of enhancing the production of energy and ECM in the IVD by implanting porous mass transfer devices through the AF.

ATP not only serves as an energy source but also a building block for PG biosynthesis [23, 24]. The activities of maintenance and repair of articular cartilage ECM are strongly associated with cell energy storage while the ECM biosynthesis rates are closely related to the availability of ATP [135, 136]. Johnson et al. has reported that intracellular ATP levels decline during the development of spontaneous knee osteoarthritis in guinea pigs, indicating that depletion of ATP is associated with cartilage degeneration [137]. Furthermore, our previous study showed that extracellular ATP promotes the ECM production of IVD cells in agarose gel culture [29]. Those results suggested that ATP production may play an important role in maintaining the healthy ECM structure of the IVD. In this study, with the implantation of PU mass transfer device, the ATP and PG contents were found to be significantly increased at NP region, suggesting that implanting porous mass transfer devices can promote nutrient transport and enhance ATP and ECM production, which has the potential to slow down disc degeneration.

Glycolysis is the process that the cells breakdown glucose into pyruvate and produce ATP. During aerobic conditions, pyruvate enters the mitochondria and more ATP is produced by the Krebs cycle and the electron transport chain. In the anaerobic respiration pathway, pyruvate is oxidized into lactate without ATP production. Previous studies have suggested that ATP is predominantly generated in IVD cells by glycolysis due to hypoxic conditions in the IVD [14, 19, 48]. In this study, both ATP and lactate contents were found to be significantly higher at the peripheral NP region in the device group compared to the intact group, suggesting that the increase in ATP content results from the augmentation of the glycolysis process. In addition, the glucose consumption rate can be described by the Michaelis-Menten Kinetics [48] in which the glucose consumption is highly sensitive to glucose concentration at low glucose levels. It explains that the device group exhibited 2.7 fold higher ATP content with only a slight increase in glucose concentration compared to the intact group.

Previous animal studies showed that needle puncture injury significantly altered the mechanical properties of the IVD and resulted in degenerative changes when the ratio of the needle diameter to disc height is greater than 0.4 [138-140]. A large needle puncture may cause the change of mechanical behaviors of IVD by damaging the AF structure and depressurizing the NP. Changes in the mechanical microenvironment may also result in degenerative responses in IVD cells, such as catabolic, apoptotic and inflammatory activities [141-144]. In this study, the ratio of the needle diameter to disc height was greater than 0.4. When comparing the structural stiffness and disc height among experimental groups after 7 days of culture, significant reductions in disc height and structural stiffness were found in the surgical group which had defects created in the AF

without implantation of mass transfer devices. The findings of the loss of disc height and structural stiffness are consistent with previous studies [35, 138]. In the device group, there was some loss of height, but this has minimal compared to the surgical groups. Therefore, proper repair of AF structural damage could maintain the mechanical function of the IVD and prevent or slow the development of disc degeneration. Likhitpanichkul et al. has demonstrated on bovine IVDs that sealing large AF defects by fibrin-genipin hydrogel can diminish the NP depressurization and restore the integrity of the AF structure [35]. Similarly, in our study, the PU mass transfer device serves a sealant or plug which repairs AF damage caused by the impanation procedure and maintains the mechanical function of the IVD.

Since there is generally an inverse relationship between the mechanical and transport properties of porous materials [129], seeking the balance between those properties is the key to developing mass transfer devices for the IVD. In our previous study, the mechanical and mass transport properties of the PU mass transfer device have been systematically characterized [129]. With the current fabrication protocol, the compressive modulus of the PU mass transfer device is about 0.15 MPa which is similar to the aggregate modulus of porcine AF tissue [145]. Since an AF defect can alter the local mechanical environment [146], which may have a negative influence on IVD cells at the defect region [141], one of the design criteria of biomaterials for repairing IVD is mechanical similarity to native IVD [128]. Therefore, with the mechanical strength similar to the AF, the PU mass transfer device used in this study may minimize the mechanical effects of an AF defect on IVD cells. In addition, the permeability and glucose diffusivity of the PU mass transfer device are about 10^6 and 5 times higher than

intact AF tissue respectively [93]. With a higher diffusivity, the PU mass transfer device provides a minimally restricted route for nutrients to diffuse into the IVD, which is shown in this study. Also, dynamic compressive loading can promote solute transport in the IVD [147]. By taking advantage of IVD mechanical loading conditions, such load-enhanced transport mechanism may further promote nutrient delivery via implanted deformable permeable passive mass transfer devices. Therefore, with proper mechanical and transport properties, the PU mass transfer device could prevent detrimental changes in the mechanical environment of IVD cells due to defects and also facilitate nutrient supply to maintain the biological function of IVD cells.

Previous studies have shown promising results in the biological treatments in degenerated disc such as with cell transplantation or with the injection of growth factors [57, 62, 148-150]. However, most of the previous studies used small animals which cannot simulate the conditions of nutrient loss in degenerated human IVDs. The main purpose of the biological treatments (e.g., injection of growth factors and/or cells) is to promote ECM production and to increase cell proliferation [63, 66]. Therefore, the biological treatments will increase the demand for nutrients and worsen the conditions of nutrient loss or low ATP concentration in the disc or NP. The mass transfer device can be used to provide additional nutrient supply during novel biological treatments. Hence, utilizing PU mass transfer devices may help supplement the biological treatments for degenerated discs to achieve successful outcomes.

One of the limitations in the current study is that only the compressive stiffness was evaluated for the mechanical function of the IVD. Since bending and twisting are two additional important motions to study spine segments, further experiments are needed to

investigate the tensile and torsional biomechanical behaviors. In addition, since the biomechanical and biochemical responses of healthy and degenerated discs to needle punctures may be different, the findings of this study need to be further verified with degenerated discs. Furthermore, distribution of nutrients in the disc was size dependent. To have a consistency of disc size, only three FSUs from L2 to L5 were utilized for the experiments which limited the number of control groups in our study. Different control groups such as with implantation of non-porous devices or without bone cement sealing will be considered in our future studies. The implantation site of PU mass transfer device was from the dorsal side of AF region which is similar to the location of entry through the AF during the lumbar discogram procedure. One could use a percutaneous procedure similar to a discogram to insert the PU mass transfer devices through the dorsal AF in discs demonstrating degeneration to attempt to arrest disc degeneration from nutrient loss. During daily living, the human lumbar spine withstands compressive loads of high magnitudes [151] which may cause migration and deformation of implanted devices [34]. In this study, no static or dynamic loading was applied to FSUs during 7 days of culture. Therefore, future long term studies are needed to examine the effects of physiological compressive loading on PU mass transfer devices as well as potential integration between tissue and device.

4.5 Conclusion

In summary, this study demonstrated the enhancement of energy (ATP) and ECM production in the IVD by utilizing the PU mass transfer devices. In addition, the compressive stiffness and height of the IVD were not affected by implantation of PU mass transfer devices after 7 days of culture. Placing the PU mass transfer device helped to slow loss of disc height when compared to the surgical groups with AF defects only. The results of this study will help in the development of novel treatment strategies for disc degeneration.

Chapter 5: Quantitative Analysis of Glucose Distribution in Porcine Intervertebral Disc with Mass Transfer Device

5.1 Introductory Remarks

As mentioned in previous chapters, IVD is the largest avascular tissue in the human body and two nutrient transport routes have been introduced [5, 6] . Essential nutrients are delivered by diffusion and convection through dense ECM over a long distance to the NP region from the blood supply at either the margin of the AF or the vertebrae. The lower level of oxygen and glucose compared to levels in the bloodstream has been measured in the center of the disc [21, 147]. Nutrients from vertebrae blood vessels are delivered through endplate often calcified with aging, further reducing the nutrient level in the NP region. Maintaining normal cellular function, (e.g., ECM biosynthesis) is crucial to retain tissue integrity [23, 24, 152-154]. Reduction in nutrient transport into the IVD may be detrimental to cell viability and facilitate disc degeneration [19, 155]. Poor nutrient supply has been considered as one of the important factors of the IVD degeneration. Therefore, understanding the glucose distribution in the IVD can help the development of potential treatment for disc degeneration.

Several mass transfer devices, such as microporous catheters, have been used for drug delivery and hemodialysis [30-33]. The purpose of transfer devices is to either remove cellular metabolic wastes from or deliver therapeutic compounds to the body based on the principle of diffusion of solutes across a semi-permeable membrane. In the IVD, similar devices could be used to deliver essential nutrients and remove metabolites. The effects of PU mass transfer device on the porcine model have been examined in our previous chapter. However, the design of the PU mass transfer device has not been optimized.

The advantage of utilizing of a theoretical model is reducing trial and error process and reducing the cost of animal experiments. The theoretical models developed based on the mechano-electrochemical mixture theory have been used to successfully describe the physical and chemical signals in the IVD [156-158] as well as to characterize the cellular metabolism of nutrients [147]. The mathematical modeling and simulation can help optimize the design of the mass transport devices by analyzing the cellular metabolism of the IVD when implanted with the devices. Therefore, the objectives of this chapter are to (1) validate the theoretical model of the mechano-electrochemical mixture theory using the organ culture of porcine IVD and (2) theoretically analyze the effects of PU mass transfer devices of different designs on the glucose distribution and consumption in porcine IVD.

5.2 Materials and Methods

Organ culture of porcine IVD

The FSUs were harvested as described in Chapter 4. After the isolation and washing process, the FSUs from each pig were randomly divided into intact and device groups, and the sectioned planes of vertebrae were sealed with bone cement. For the device group, two puncture holes (diameter smaller than 2.5 mm) were created bilaterally using sterile needles at the dorsal side of the AF region without removing tissue. The PU mass transfer devices were squeezed and implanted under a press-fit condition. Both intact and device groups were cultured in low glucose (1g/L) DMEM containing 1% of antibiotic-antimycotic and 50 µg/ml of gentamicin sulfate at 37°C, 5% CO_2, and 20% O_2 within an incubator. After 7 days of culture, a transverse cut was made at the mid-disc height of the

FSUs to expose the NP and the AF regions. Tissue samples (~25mg) were harvested from three different locations (AF, peripheral NP and central NP regions) along PU mass transfer devices in the device group and the same locations in the intact group.

Glucose measurement

The glucose measurement has been described in chapter 4. In brief, tissue samples (n=8) harvested from the intact and device groups were digested by the papain method and the glucose concentration was measured using a glucose (GO) assay kit. Measurement of tissue density was described in chapter 4 glucose measurement section for the calculation of tissue volume. Glucose concentration was calculated by dividing the glucose content by tissue volume.

Measurement of cell density in the porcine IVD

Tissue samples (~25 mg) from the NP and the AF regions (n=4 for each region) were harvested from Yorkshire pigs within 2 hours sacrifice. The tissues samples were digested with papain and the DNA content of each sample was measured by the Hoechst 33258 fluorometric assay. In order to convert DNA content into cell number, the relationship between the DNA content and the number of IVD cells was established. Some tissue samples were enzymatically digested in DMEM containing 1 mg/mL collagenase type II (Worthington Biochemical Corp., Carlsbad, CA) and 0.6 mg/mL protease (Sigma) for about 24 hours at 37 °C and 5% CO_2. AF tissue required to break down mechanically using a syringe to facilitate tissue digestion while in its respective digestion solution. The mixtures containing cells were filtered using a 70 µm strainer

(BD Bioscience, San Jose, CA) to remove undigested tissue. The cells were cultured under high glucose DMEM supplemented with 10% of fetal bovine serum (Corning, Amsterdam, Netherlands) and 1% of antibiotics. While the culture reached the full confluency, the cells were trypsinized and calculated by the hemocytometer (Hausser Scientific, Horsham, PA). After papain digestion, the DNA content of IVD cells was measured by the Hoechst 33258 fluorometric assay. Two million IVD cells were utilized to determine the ratio of cell number to DNA content which was used to determine the number of cells in tissue sample. Tissue volume was determined as described in chapter 4 glucose measurement section. The cell density of porcine NP and AF was calculated by dividing the cell number by the tissue volume.

Theoretical model

The theoretical framework of the mixture theory reported previously [147] was used to quantitatively analyze the transport and consumption of glucose and oxygen in the IVD. The IVD tissue was considered as a mixture of an elastic, porous, permeable solid phase, an interstitial fluid phase, and five solute phases (i.e. sodium and chloride ions, oxygen, glucose and lactate). For the IVD, the metabolic rates of sodium and chloride ions were assumed to be zero. The consumption rate of oxygen and glucose by IVD cells were pH and concentration dependent as described previously [159]. The consumption rate of oxygen (Q^{o_2}) was described as [147]:

$$Q^{o_2} = -\frac{V'_{max}(pH - 4.95)c^{o_2}}{K'_m(pH - 4.59) + c^{o_2}}\rho^{cell}$$

Where V'_{max} was the maximum consumption rate of oxygen, K'_m was the Michaelis-Menten constant for oxygen, c^{o_2} was the concentration of oxygen (kPa) and ρ^{cell} was the

cell density of tissue. The lactate production rate of IVD cells ($Q^{lactate}$) was given as [159]:

$$Q^{lactate} = \exp(-2.47 + 0.93 \times pH + 0.16 \times c^{o_2} - 0.0058$$

$$\times c^{o_2^2})\rho^{cell} \frac{c^{glucose}}{(K_m^l + c^{glucose})}$$

Where K_m^l was the Michaelis-Menten constant for lactate and $c^{glucose}$ was the concentration of glucose (mM). The ratio between lactate production and glucose consumption was assumed to be 2.0 [14, 160]. The theoretical glucose consumption rate of AF cells was set 4 times lesser than the NP cells based on a previous study [161]. The relationships between pH and lactate concentration reported in previous studies [14, 147, 162] were used to determined pH within the IVD. The solid matrix in the IVD was assumed to be a negatively charged isotropic material. Strain-dependent properties (fixed charge density, solute diffusivities, hydraulic permeability and volume fraction of water) were considered for the IVD in the simulation [107, 110, 156, 157].

The mass transfer device used in this study was a porous cylinder which allowed solutes exchange and provides mechanical support. The device was filled with water and solutes. Thus, the mass transfer device was also considered as a mixture of an elastic solid phase, a fluid phase and five solute phases as described above. The solid phase of the device was assumed to be a non-charged isotropic material. The glucose diffusivity and hydraulic permeability of mass transfer device were determined in chapter 3. The other solutes diffusivities were estimated using Stokes-Einstein equation which the diffusivity was inversely proportional to the solutes radii [163]. The metabolic rate of all solute phases was assumed to be zero in the device. The porosity of the device was examined in the previous chapter which is 68%.

The vertebral body was a porous structure which composed by cortical and cancellous bone. It was also filled with water and solutes, and considered as a mixture of an elastic solid phase, a fluid phase and five solute phases. The solid phase of the vertebrae was assumed to be a non-charged isotropic material. The relative diffusivity of solute in the cortical bone was estimated using the fiber matrix theory [163]: $\frac{D_{cortical}^{\alpha}}{D_0^{\alpha}} = \exp\left[-\sqrt{V_f}\left(1 + \frac{r_s^{\alpha}}{r_f}\right)\right]$ where V_f was the volume fraction of fiber (10%), r_s^{α} was the hydrodynamic radius of the solute, and r_f was the radius of the fiber (0.6 nm). Based on the fitting results from previous study, the fiber volume fraction of cortical bone was parametrically varied between 0.1 to 10% [163]. Since the pore size and porosity of cancellous bone were much larger than cortical bone, the volume fraction of fiber was assumed to be much smaller than 0.1. Hence, the solutes diffusivities in the cancellous bone were assumed to be the same as those in water. The metabolic rate of all solutes was assumed to be zero in the vertebrae. The porosity of cortical and cancellous bone was determined by the previous studies which were 30% and 95%, respectively [164, 165].

Finite element analysis

The three-dimensional porcine IVD model, which is composed of two anatomical regions, the NP and AF region, was created based on the anatomical geometry of the porcine L3-L4 lumbar (Figure 5-1a). Due to the symmetry, only the upper right quarter of the disc was analyzed (Figure 5-1b and c). The mass transfer devices with a circular cross section were implanted from the posterior region in the transverse plane at the mid-height of the IVD bilaterally based on the common lumbar discogram procedure (Figure 5-1d). The device was used to augment the nutrient level in the NP region by providing a

passage for nutrients to diffuse into the NP region from the vascularized region at the AF edge. For validation of the model, the numerical simulation was performed in two scenarios. First, the vertebrae were assumed to be impermeable, and only the IVD was included in the analysis (Figure 5-1b). Second, the vertebrae were assumed to be permeable, and the vertebrae and IVD were included in the analysis (Figure 5-1c). Since the section planes of the vertebrae were sealed by bone cement, the nutrient could diffuse from the lateral surface of the vertebrae and the AF edge to the NP. After the validation of the theatrical model, the effects of the PU devices of different sizes (device diameter: 1.5 mm, 2.5 mm and 3.5 mm) were analyzed (Figure 5-1d). The influence of AF cellular consumption on the delivery of nutrients to the NP region was also examined by blocking solute exchange in the AF portion of the devices.

The boundary condition was based on the experimental culture condition (Table 5-1). The parameters used in the numerical simulations for the healthy discs were adopted from previous studies [21, 147] and listed in Table 2. The governing equation with the initial and boundary conditions was solved using a finite element method package (COMSOL Multiphysics 4.3, COMSOL Inc., Burlington, MA). A mesh of 535 and 806 triangular elements were used in the simulations of intact and device model for the first validation scenario. For the simulations of the second validation scenario, different sizes of the device and device with impermeable AF, a mesh of 1876 and 2701 triangular elements of intact and device model with vertebrae were utilized. The convergence criterion for the solution was a relative error tolerance of less than 10^{-6}.
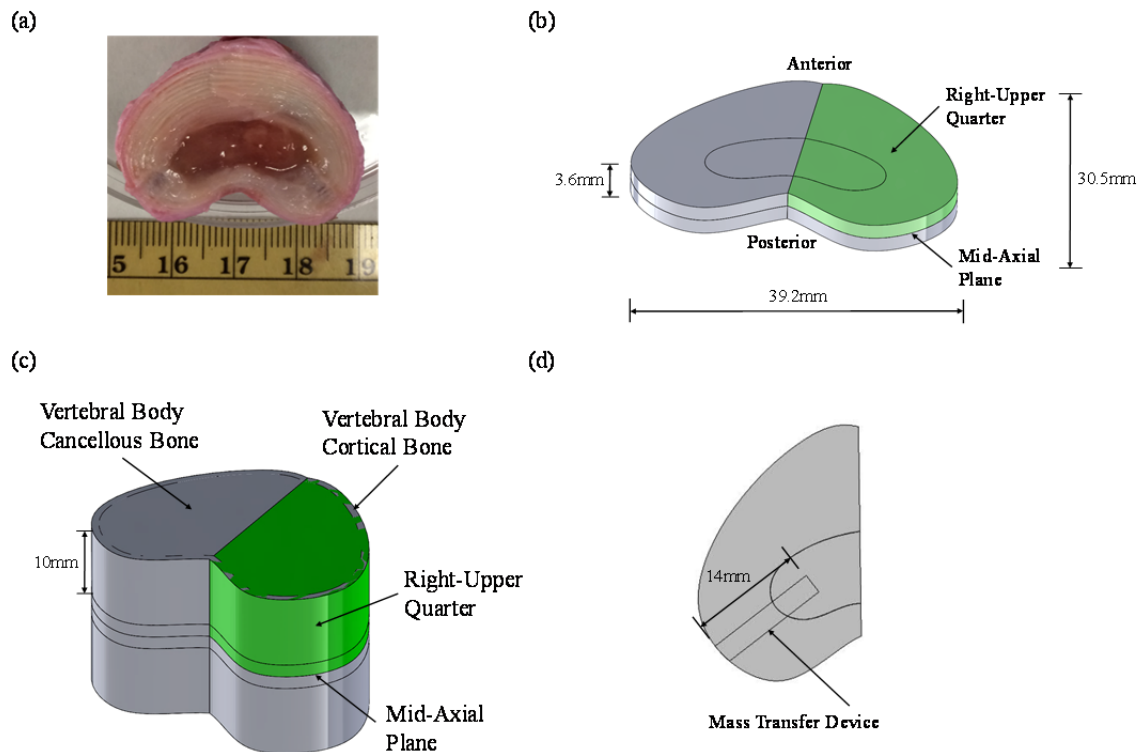
Figure 5-1. (a) Geometry and size of the disc from the porcine lumbar disc. Schematic of the right upper quarter of the disc used in the simulation (b) without and (c) with vertebral body. (d) Location of the mass transfer device implantation.

Table 5-1. Boundary condition of the IVD and the devices used in the finite element analysis

Inlet of the device at the AF edge, or At the interface between NP and AF (Device with impermeable AF)	$c^{O_2} = 20.265\ kPa, c^{glucose} = 5.5mM, c^{lactate} = 0mM,$ $c_i^{Na^+} = c_i^{Cl^-} = 150\ mM$ For all cases: $\sigma_x = \sigma_y = \sigma_z = \sigma_{xy} = \sigma_{xz} = \sigma_{yz} = 0$
The interface between AF and the device	Device with impermeable AF: $J^{Na^+} = J^{Cl^-} = J^{O_2} = J^{lactate} = J^{glucose} = 0$ $\sigma_x = \sigma_y = \sigma_z = \sigma_{xy} = \sigma_{xz} = \sigma_{yz} = 0$
At the AF edge, and The lateral surface of vertebrae	$c^{O_2} = 20.265\ kPa, c^{glucose} = 5.5mM, c^{lactate} = 0mM,$ $c_i^{Na^+} = c_i^{Cl^-} = 150\ mM$ For all cases: $\sigma_x = \sigma_y = \sigma_z = \sigma_{xy} = \sigma_{xz} = \sigma_{yz} = 0$
At the endplate, or At the bone cement region	$c^{O_2} = 0\ kPa, c^{glucose} = c^{lactate} = c_i^{Na^+} = c_i^{Cl^-} = 0\ mM$ For all cases: $\sigma_x = \sigma_y = \sigma_z = \sigma_{xy} = \sigma_{xz} = \sigma_{yz} = 0$
At the mid-height (z=0)	$J_z^{water} = J_z^{Na^+} = J_z^{Cl^-} = J_z^{O_2} = J_z^{lactate} = J_z^{glucose} = 0$ $u_z = 0, \sigma_{yz} = 0, \sigma_{xz} = 0$
At the disc center (x=0)	$J_x^{water} = J_x^{Na^+} = J_x^{Cl^-} = J_x^{O_2} = J_x^{lactate} = J_x^{glucose} = 0$ $u_x = 0, \sigma_{zx} = 0, \sigma_{yx} = 0$

Note: u_i is the displacement in i-direction, σ_{ij} is the stress in j direction on the surface with a normal along the direction i, J^i is the flux of the solute i.

Table 5-2. The parameter of the IVD and the device used in the numerical analysis

	Water Content	Elastic constant (kPa)	Fixed charge density (M)[21]	Constitutive equation of diffusivity	Constitutive equation of hydraulic permeability
AF	75%	$\lambda = 300$ [21] $\mu = 100$	0.15	A=1.29[*] B=0.375[*]	a=0.00044nm^{2}[#] n=7.1929[#]
NP	86%	$\lambda = 15.6$ [21] $\mu = 0.18$	0.25	A=1.25[*] B=0.681[*]	a=0.00339nm^{2}[#] n=3.24[#]
Device	68%	Same as AF region	0	Glucose diffusivity was determined in previous chapter: 5.01×10^{-10} m^{2}/s, The other solutes were estimated by Stroke-Einstein equation[&]	Determined in previous chapter: 2.86 ×10^{-9} m^{4}/Ns
Vertebrae	Cortical [164]: 30% Cancellous [165]: 95%	Cortical [166]: 4000×AF Cancellous[166]: 40×AF	0	Cortical[163] : The solutes diffusivity was estimated using the fiber matrix theory[$] Cancellous [163]: $\frac{D_{cancellous}^{\alpha}}{D_0^{\alpha}} = 1$	Assume same as the Device

[*]Tissue Diffusivity (D_{tissue}^{α}) of solute α was estimated using the constitutive equation: $\frac{D_{tissue}^{\alpha}}{D_0^{\alpha}} = exp\left(-A\left(\frac{r_s^{\alpha}}{\sqrt{k\eta}}\right)^B\right)$ where D_0^{α} was the solute diffusivity of solute α in aqueous solution ($D_0^{O_2} = 3\times10^{-9}\frac{m^2}{s}, D_0^{lactate} = 1.28\times10^{-9}\frac{m^2}{s}, D_0^{glucose} = 9.2\times10^{-10}\frac{m^2}{s}$), r_s^{α} was the hydrodynamic radius of solute $r_s^{O_2} = 0.1nm, r_s^{lactate} = 0.255nm, r_s^{glucose} = 0.3nm, k$ was the hydraulic permeability, η was the viscosity of water, and A and B were the material constants [147].

[#]Hydraulic permeability (k) was estimated using the constitutive equation: $k = \frac{a}{\eta}\left(\frac{\phi^w}{1-\phi^w}\right)^n$ where a and n were material constants and ϕ^w was the tissue porosity [167].

[&]The solutes diffusivities (other than glucose) of the device were estimated using Stokes-Einstein equation: $D^\alpha_{device} = \frac{k_B T}{6\pi\eta r_s^\alpha}$ where k_B was the Boltzmann constant, T was the room temperature [163].

[$]The relative diffusivity $\left(\frac{D^\alpha_{cortical}}{D^\alpha_0}\right)$ of cortical bone was estimated using the fiber matrix theory: $\frac{D^\alpha_{cortical}}{D^\alpha_0} = \exp\left[-\sqrt{V_f}\left(1 + \frac{r_s^\alpha}{r_f}\right)\right]$ where V_f was the volume fraction of fiber (10%) and r_f was the radius of the fiber (0.6 nm) [163].

5.3 Results
Comparison of glucose concentration between experimental and theoretical model

The cell density of porcine NP and AF tissue was examined and utilized for the simulation. The cell density of NP region was less than that of the AF region (8710 and 32600 cells/mm^3 for NP and AF, respectively). Two different scenarios were performed for the simulation. In the first scenario, the vertebrae were assumed to be impermeable and the nutrients were only diffused from the AF edge. With the adjustment by 20% of the cellular metabolic rate of lactate, the experimental glucose concentration in the device and intact groups at central NP, peripheral NP and AF could be matched with the simulation results (Figure 5-2). In the second scenario, the vertebrae were assumed to be permeable and nutrients were diffused from the lateral surface of vertebrae and AF edge. The theoretical simulation demonstrated a good agreement with experiment results without any adjustment of cellular metabolic rate (Figure 5-3).

The effect of device size

Since the second scenario provided a better prediction of glucose concentration, the model with the second scenario was utilized for the further mass transfer device analysis. The augmentation of the concentration and consumption rate of glucose depended on the size of the device (Figure 5-4). By increasing the diameter of the device from 1.5 mm to 3.5 mm, the glucose concentration and the consumption rate at the center point of the NP region increased 2.2 % and 1.52 %, respectively. The augmentation of glucose concentration was not uniform in the NP, with the location at a longer distance from the device exhibiting less effect.
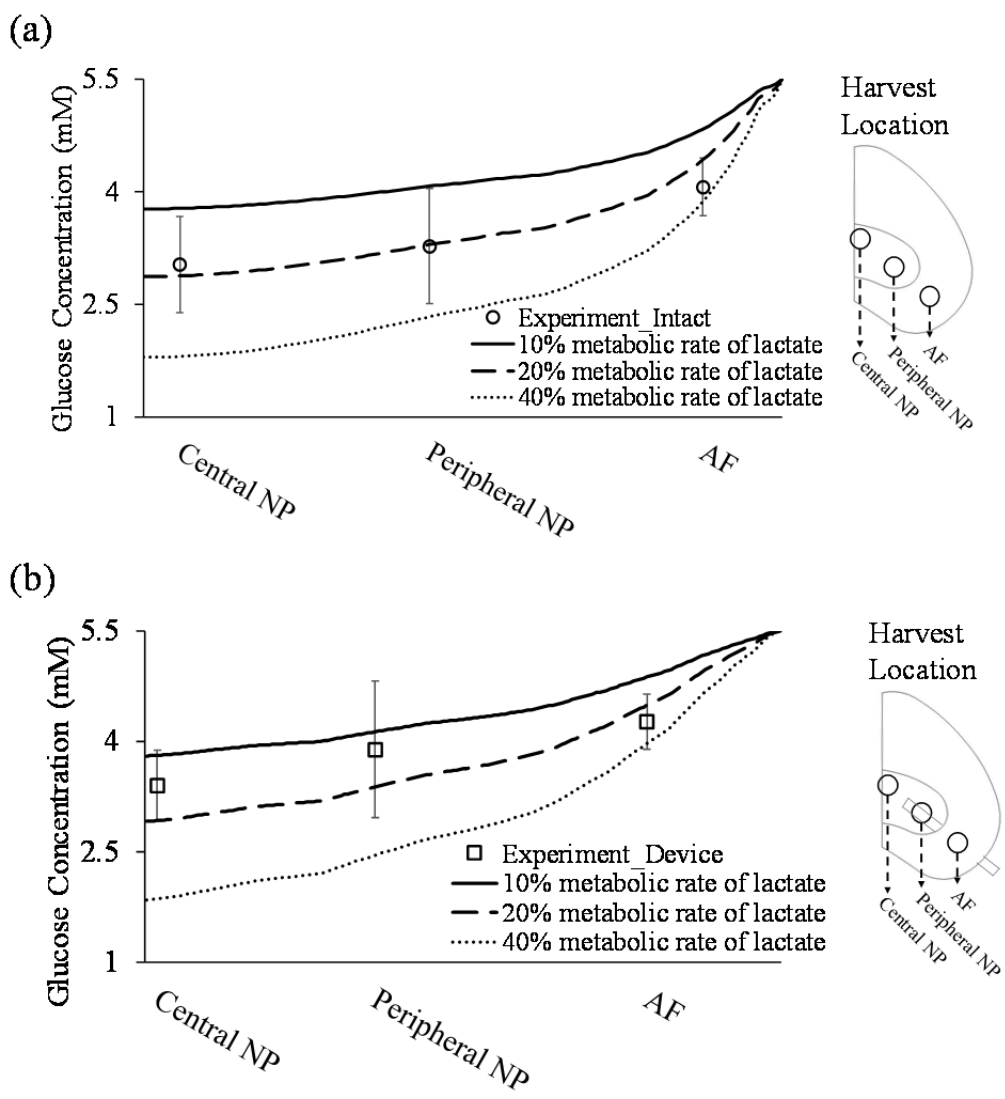
Figure 5-2. The comparison of glucose concentration distribution between experimental and theoretical model in (a) intact and (b) device group at the mid-height of the disc with different percentage of the cellular metabolic rate of lactate.
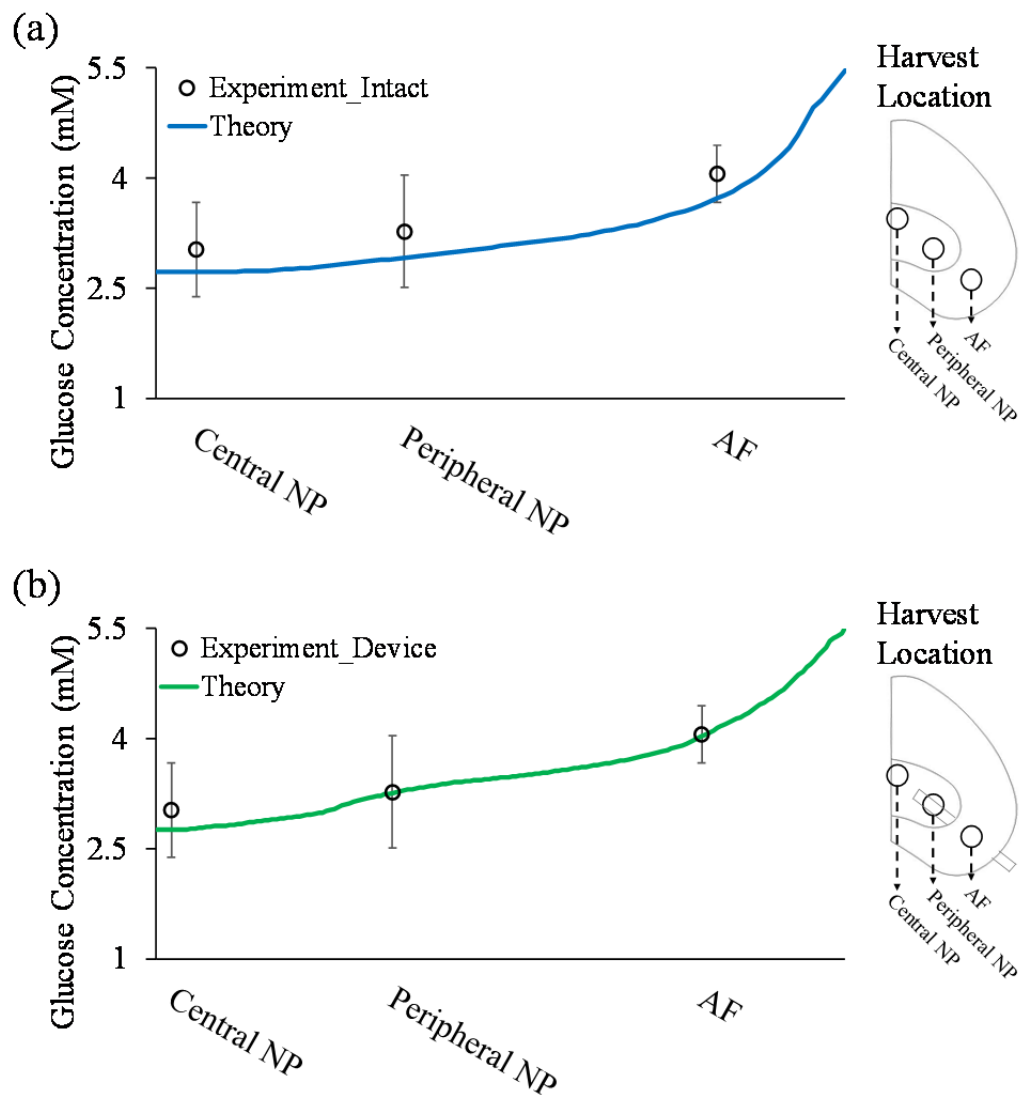
Figure 5-3. The comparison of glucose distribution between experimental and theoretical model in (a) intact and (b) device group at mid-height of the disc with vertebral body permeable.

(a)

(b)
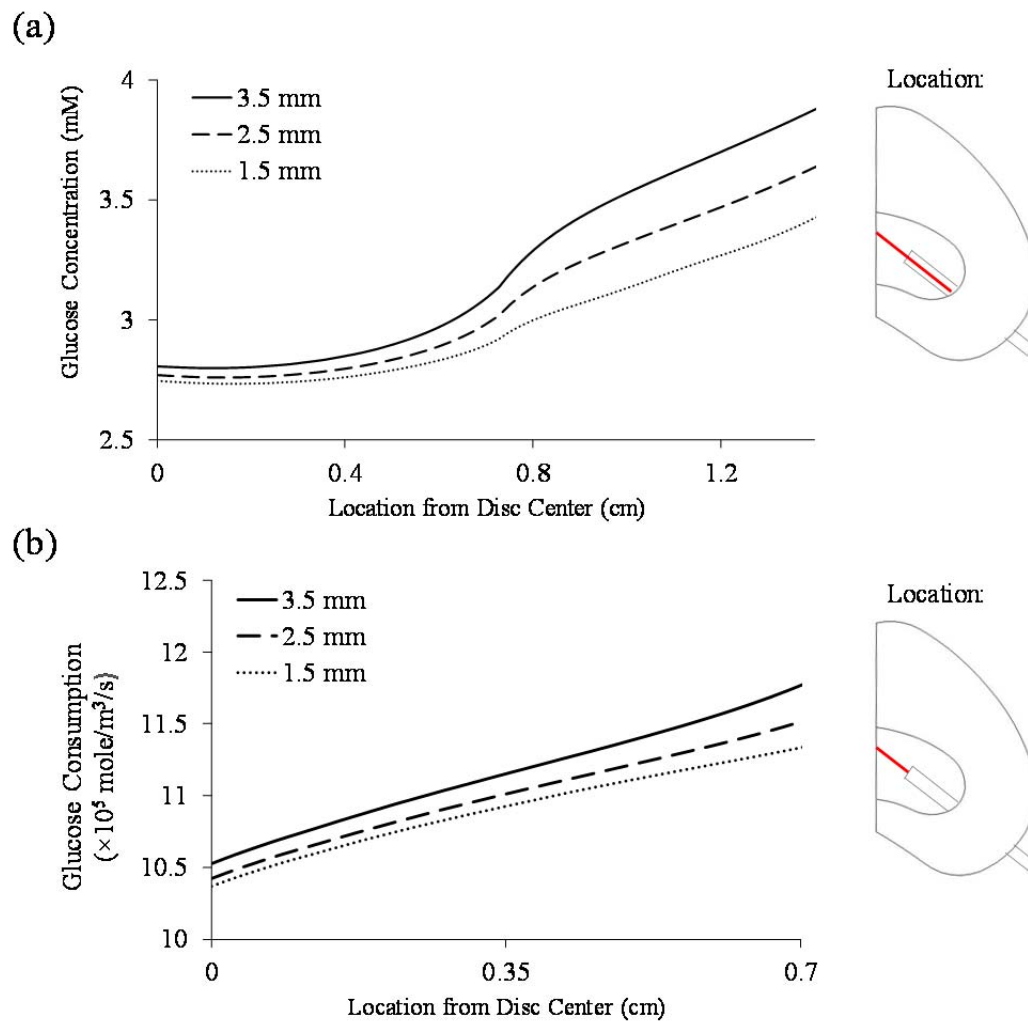
Figure 5-4. Comparison of the distribution of (a) glucose concentration and (b) consumption rate at the mid-height of the disc with the implantation of the mass transfer device with different diameter sizes.

The effect of mass transfer device with impermeable AF portion

The mass transfer device with 2.5 mm diameter was utilized for the simulation of mass transfer devices with impermeable AF portion. Since the AF cells consumed certain amounts of glucose, blocking the nutrient exchange between the device and the AF region may further enhance the transport of nutrients into the NP region (Figure 5a and b). When comparing the glucose concentration at the center point of the NP region, the device of both designs (with impermeable AF and permeable AF regions) showed similar glucose levels (Figure 5c). However, the average glucose concentration of the whole NP region was about 2 % higher in the IVD implanted with the AF impermeable device than the AF permeable device. When comparing the augmentation level of glucose consumption rate, the AF impermeable device was 3.1 times higher than the AF permeable device (Figure 5d).

5.4 Discussion

This study quantitatively analyzed the glucose distribution of porcine IVD experimentally and theoretically. The model of the mechano-electrochemical mixture theory was validated by the good agreement between experimental and theoretical results. In addition, the mass transfer device with larger size and impermeable AF portion could be the best design to promote the transport of nutrients into the NP region.
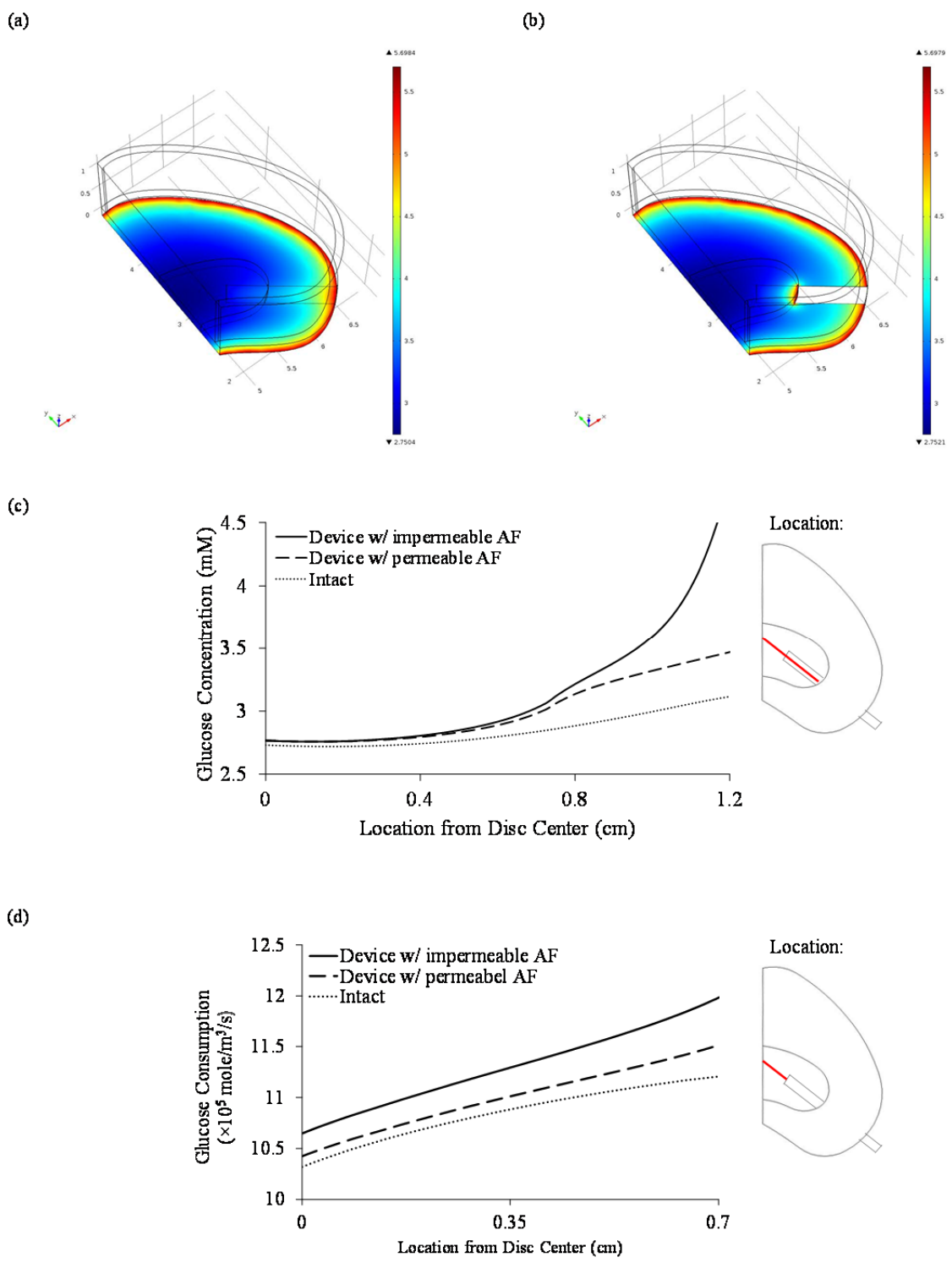
Figure 5-5. Distribution of glucose concentration at mid-height of the disc of the device with (a) permeable and (b) impermeable AF. The comparison of (c) glucose concentration and (d) consumption rate of the intact and device with permeable AF and impermeable AF.

In our previous study, the theoretical simulation of glucose distribution in human IVD with the same production rate of lactate in NP and AF cells has been investigated, and a sharp decrease of glucose concentration was found in the AF region [21] which was not consistent with our experimental results. Therefore, the adjustment of the AF glucose consumption rate has been applied to the simulation based on Jackson's study [161]. The differences in the cellular metabolic rate between NP and AF cells have been reported in previous studies [161, 168-170]. Holm et al. showed that the lactate production rate of NP cells from adult Labrador dogs was higher than the AF cells [168]. Ishihara et al. found that NP cells from bovine coccygeal IVD exhibited higher oxygen consumption rates than AF cells under high oxygen tension [169]. Similar results of porcine IVD cells were also reported by our previous study [170]. The difference of cellular metabolic rate of NP and AF cells may due to difference cellular phenotypes. As mentioned in the previous chapter, NP was arising from notochord and AF was from mesenchyme which results in different cell morphology, phenotypic expression and matrix production [43]. In our study, with the adjustment of the AF glucose consumption rate, the glucose concentration gradually reduced from AF to the center NP which was more similar to the experimental measurements.

Two different scenarios have been proposed in this study in order to determine proper boundary conditions by matching the theoretical and experimental results. In the experimental conditions, the cut ends of the vertebrae were sealed with bone cement in order to block the nutrient pathway through the endplate route. However, 10 mm height of vertebrae was still preserved on each side of the FSUs. The lateral surface of the vertebrae which was not covered by the bone cement might remain permeable. The

nutrients might diffuse from the lateral surface of the vertebrae into the NP region. In the simulation results, the permeable vertebrae model showed a better agreement between the theoretical and experiment results without adjustment of the cellular metabolic rate. However, the experimental glucose concentration in the intact group was still slightly higher than the theoretical simulation. The variation might be due to the differences in experimental animals and the condition of metabolic rate measurement. The production rate of lactate, as well as the consumption rate of glucose, used in this study was based on the results of bovine NP cells [14], which was different than our experiment animal. In addition, the cellular metabolic rates for the simulation model were measured from isolated IVD cells which might present different metabolic rates than the cells in *in situ* condition.

In this study, the simulation results demonstrated that with a larger size of mass transfer device, a better augmentation of nutrient levels in the NP region could be achieved. Based on the previous results from chapter 4, with the implantation of PU mass transfer devices, the compressive stiffness and height of the IVD could be preserved after 7 days of culture. Although the ability of maintaining mechanical properties of the IVD by the PU mass transfer device has been approved, a larger size of the device also represented a larger AF defect. Therefore, further biomechanical testing is needed to confirm the safety and the feasibility to prevent the detrimental changes in the mechanical environment of IVD cells with the implantation of a larger PU mass transfer device.

Based on the experimental and theoretical results, the mass transfer device with permeable AF portion could promote diffusion of nutrients into the NP region. However,

AF cells consumed certain amounts of glucose from the mass transfer device. Therefore, blocking the nutrient exchange at the AF region could enhance nutrient transport into the NP region as demonstrated in this study. The simulation results demonstrate that the device with impermeable AF region could increase the glucose concentration and the glucose consumption rate at the NP region. With the optimized design of the mass transfer device and the implantation of multiple devices for better nutrient augmentation, it may provide another potential option of treating degenerated discs.

In this study, the theoretical simulation was validated by the experimental results which could help the future development of mass transfer device. Since the load-enhanced transport mechanism may promote nutrient delivery via the mass transfer device [147], mechanical loading could be applied in the theoretical model. The nutrient distribution in the IVD was disc size dependent, and the size difference could be found between human and porcine IVD. With the difficulties of performing the experiments in human subject, the theoretical model could be utilized for evaluating the effect of PU mass transfer device in human IVD under degeneration condition.

In the results of glucose distribution of the mass transfer device group, the glucose concentration decreased sharply from the end of the mass transfer device to the center of NP. The enhancing of glucose concentration was not uniform in the NP region, and the location with longer distance from the device exhibited a lesser effect of nutrient augmentation. Therefore, the extending length of the device might increase the nutrient level in the center of the NP region.

5.5 Conclusion

In summary, this chapter demonstrated that the theoretical model used in this study could predict the experimental glucose distribution in intact and device groups. In addition, the device with the larger size and impermeable AF region could increase the nutrient level in the NP region. The results of this study could help the future development and design of novel treatment strategies for disc degeneration.

Chapter 6: Conclusion and Recommendation for Future Work

6.1 Summary and Concluding Remarks

Low back pain is a common physical condition which affects up to 85% of people during their lifetimes and costs billions of US dollars per year in healthcare in the United States. All the causes of the low back pain remain to be elucidated [1, 2]. However, IVD degeneration has been considered relevant to the cause of low back pain [5]. Since IVD is the largest avascular tissue in the human body, the nutrient supply is the key to preserving the viability and functionality of the IVD [6]. With the reduction of the nutrient supply, there is decreased ECM production and this may cause cell death. Poor nutrient supply has been suggested as one of the important factors in disc degeneration [10].

Cell activities such as ECM production and maintenance of the IVD are high energy demanding processes which required ATP as fuel [22]. ATP also serves an important role in the formation of PG and as an extracellular signaling molecule [24, 29]. Since ATP is important for maintaining the integrity and functionality of the IVD, insufficient ATP levels may lead to cell death and IVD degeneration.

The utilization of a mass transfer device for drug delivery and hemodialysis has been demonstrated [30-33]. The purpose of the mass transfer device is to remove cellular metabolic waste or deliver therapeutic drugs to the body by the principle of diffusion of solutes across a semi-permeable membrane. The similar concept could be applied to the IVD. Since there are ample nutrient supplies at the AF edge due to the blood supply, the mass transfer device could be utilized for facilitating the nutrient transport from the AF edge to the NP region. Therefore, investigating the enhancement of nutrient and energy

87

levels in the IVD with the implantation of PU mass transfer device may help in the development of new treatment strategies for IVD degeneration and low back pain.

The main objectives of this dissertation were threefold: (1) to systemically investigate the mass transport and mechanical properties of the porous PU scaffold and their relationship with porosity, (2) to investigate the enhancement of ATP production in the IVD by the implantation of porous PU scaffolds in the AF as a passive mass transfer device and (3) to validate the theoretical model of the mechano-electrochemical mixture theory using the organ culture of porcine IVD and theoretically analyze the effect of the PU mass transfer device with different designs on glucose distribution in the IVD. In order to achieve these aims, the following studies were carried out: (1) measurements of tensile modulus, compressive modulus, hydraulic permeability and glucose diffusivity of porous PU scaffolds with different PU concentrations and salt/PU weight ratios as functions of porosity (Chapter 3), (2) measurements of ATP, lactate, PG and mechanical properties of the IVD with the implantation of PU mass transfer devices in the porcine model (Chapter 4) and (3) comparison of glucose concentration distribution between the theoretical model and the organ culture of porcine IVD and theoretical analysis of the glucose concentration and consumption rate with different sizes of mass transfer devices and devices with impermeable AF portion (Chapter 5). The most important findings from these investigations are discussed as follows:

6.1.1 Characterization of porosity and mass transport and mechanical properties of porous PU scaffolds

The relationship of porosity and mass transport and mechanical properties of porous PU scaffolds were investigated. The porous PU scaffolds were fabricated by the

combination of phase inversion and the salt leaching method. The tensile and compressive moduli were examined on PU scaffolds fabricated with different PU concentrations and salt/PU weight ratios. The mass transport properties of PU scaffolds including hydraulic permeability and glucose diffusivity were also measured.

The results demonstrated that porosity is a key parameter which governs both mass transport and mechanical properties of porous PU scaffolds. With similar pore sizes, mass transport and mechanical properties of PU can be described as single functions of porosity regardless of initial PU concentration. The relationships between scaffold porosity and properties can be utilized to facilitate porous PU scaffold fabrication with specific mass transport and mechanical properties. The systemic approach established in this study can be applied to the characterization of other biomaterials for scaffold design and fabrication

6.1.2 Enhancement of energy production of the intervertebral disc by the implantation of PU mass transfer device

The porcine FSUs were used and divided into intact, device and surgical groups. For the device and surgical groups, two puncture holes were created bilaterally at the dorsal side of the AF region and the PU mass transfer devices were only implanted into the holes in the device group. Surgical groups were observed for the effects of placing the holes through the AF only.

After 7 days of culture, the surgical group exhibited a significant reduction in the compressive stiffness and disc height compared to the intact and device groups, whereas no significant differences were found in compressive stiffness, disc height and cell viability between the intact and device groups. ATP, lactate and PG contents in the

device group were significantly higher than the intact group. These results indicated that the implantation of the PU mass transfer devices can promote nutrient transport and enhance energy production without compromising mechanical and cellular functions in the disc. These results also suggested that compromising the AF has a negative impact on the IVD and must be addressed when treatment strategies are considered. The results of this study will help guide the development of potential strategies for disc degeneration.

6.1.3 Quantitative analysis of glucose distribution in porcine IVD with mass transfer device

The comparison of glucose distribution between the theoretical model and the organ culture porcine IVD was investigated. The effects of mass transfer devices of different designs on glucose concentration and consumption rate in the IVD were also theoretically analyzed. For the experimental glucose measurement, the porcine FSUs were divided into intact and device groups. For the device group, two puncture holes were created bilaterally at the dorsal side of the AF region and the PU mass transfer devices were implanted. The glucose distribution was determined after 7 days of culture. The theoretical model was developed based on the mechano-electrochemical mixture theory which can describe the physical and chemical signals and the cellular metabolism of nutrients in the IVD.

The results demonstrated that the theoretical model could predict the glucose distribution measured experimentally in intact and device groups. In addition, the theoretical analyses showed that enhancement of nutrient transport by implantation of the mass transfer device was increased by increasing device size as well as blocking the solutes exchange in AF portion. The theoretical model could be used to optimize the

design of the mass transfer device and also help the development of potential treatment strategies for disc degeneration.

6.2 Recommendation for Future Work

The overall objective of this research was to investigate the relationship between porosity and mass transport and mechanical properties of porous PU scaffolds, and the utilization of porous PU scaffolds as mass transfer devices for the augmentation of nutrient and energy levels in the porcine IVD. Although the studies presented in this dissertation provide valuable insights, there is still additional work left to fully understand the relationship between PU scaffold properties and porosity as well as the effects of PU mass transfer devices on the cellular metabolism and mechanical function of the IVD. Therefore, recommendations for the future work are described.

In chapter 3, the mechanical and transport properties of porous PU scaffolds and its relationship with porosity were investigated. The porosity of the PU scaffolds depended on the salt/polymer weight ratio, and the pore size was determined by the size of the salt crystals incorporated. Although the relationships between porosity and scaffold properties were investigated, the influence of pore size on scaffold properties was not examined. Pore size has been shown to affect the mechanical properties of porous scaffolds with the same porosity [125, 126]. In addition, the relationships between pore size and scaffold permeability and molecular diffusivity have also been mentioned in previous studies [94, 116, 117]. Therefore, different pore sizes of scaffolds could be included in future studies for a more complete analysis. In addition to pore size, the other limitation of this study is the limited range of porosity. The porosity of our scaffold falls into the range from 30%

to 70%. With the current fabrication protocol, the minimum porosity of 11% can be fabricated without incorporation of salt and the plateau of maximum porosity is around 80%. Nevertheless, with the control of salt size and salt/polymer ratio, a unique combination of mass transport and mechanical properties of PU scaffolds could be created. Different combinations of salt particle sizes and the salt/polymer ratio could be considered in future studies for the need of scaffolds with higher porosity.

In chapter 4, the enhancement of energy production and maintenance of mechanical properties of IVD by the implantation of PU mass transfer device was investigated. In mechanical testing, only the compressive stiffness was examined. Since bending and twisting are two important motions for spine segment, tensile and torsional testing should also be included for the evaluation of IVD mechanical properties. In this study, relatively young and healthy pigs were utilized in the experiments. However, the biomechanical and biochemical responses of healthy and degenerated discs to needle puncture may be different, and the results of this study should be further verified with degenerated discs. In order to have a consistency of disc size, the number of the control groups was limited. However, different control groups such as implantation of non-porous devices or without bone cement sealing should be considered in future studies for further examining the effect of PU mass transfer devices. It is known that AF plug migration and deformation are major problems of similar devices in *in vivo* experiments [34]. The sign of destruction and displacement of implants might be due to the physiological loading of animal daily activities. In this study, no static or dynamic loading was applied to FSUs during the experiments. Therefore, future long-term studies are needed to evaluate the effect of physiological loading on PU mass transfer device and the integration between tissue and

the device. The purpose of biological treatment, such as using growth factors or cell injection, is to promote the ECM production and to increase the cell proliferation [63, 66] which could increase the demand for nutrients in the IVD. The synergetic effect of PU mass transfer devices and biological treatment could be examined in future studies.

In chapter 5, the validation of glucose distribution between the theoretical model and experimental results was performed. Different designs of PU mass transfer devices were also investigated. Since the cellular metabolic rate of lactate in the theoretical model was from bovine NP cells, the parameters from porcine IVD should be measured in future studies. The load-enhanced transport mechanism may promote the nutrient delivery via the mass transfer device [147]. Therefore, mechanical loading could be added in the theoretical model. Since the nutrient distribution in the IVD was disc size dependent and it is difficult to perform experiments on human IVD, the theoretical model could be utilized for evaluating the effect of the mass transfer device on human IVD and under degeneration conditions. The further optimization of the mass transfer device could also be done in future studies. The results showed that the glucose concentration was not uniformly increased in the NP region with the implantation of the mass transfer device. Different designs of the devices, including longer length, different implantation position and combination with active delivery system, could be tested.

In summary, the recommended studies would allow us to have a better understanding of the effect of the PU mass transfer device on the IVD, which can help the development of novel treatment strategies for IVD degeneration and low back pain.

Reference

1. Andersson, G.B.J., *Epidemiological features of chronic low-back pain.* Lancet, 1999. **354**(9178): p. 581-585.

2. Katz, J.N., *Lumbar disc disorders and low-back pain: socioeconomic factors and consequences.* J Bone Joint Surg Am, 2006. **88 Suppl 2**: p. 21-4.

3. Gilson, A., M. Dreger, and J.P.G. Urban, *Differential expression level of cytokeratin 8 in cells of the bovine nucleus pulposus complicates the search for specific intervertebral disc cell markers.* Arthritis Research & Therapy, 2010. **12**(1).

4. Smith, L.J., et al., *Degeneration and regeneration of the intervertebral disc: lessons from development.* Disease Models & Mechanisms, 2011. **4**(1): p. 31-41.

5. Adams, M.A. and P.J. Roughley, *What is intervertebral disc degeneration, and what causes it?* Spine, 2006. **31**(18): p. 2151-2161.

6. Gawri, R., et al., *Development of an organ culture system for long-term survival of the intact human intervertebral disc.* Spine, 2011. **36**(22): p. 1835-1842.

7. Pattappa, G., et al., *Diversity of intervertebral disc cells: phenotype and function.* Journal of Anatomy, 2012. **221**(6): p. 480-496.

8. Urban, J.P.G. and S. Roberts, *Degeneration of the intervertebral disc.* Arthritis Research & Therapy, 2003. **5**(3): p. 120-130.

9. Boubriak, O.A., et al., *Factors regulating viable cell density in the intervertebral disc: blood supply in relation to disc height.* J Anat, 2013. **222**(3): p. 341-8.

10. Horner, H.A. and J.P.G. Urban, *2001 Volvo Award winner in basic science studies: Effect of nutrient supply on the viability of cells from the nucleus pulposus of the intervertebral disc.* Spine, 2001. **26**(23): p. 2543-2549.

11. Grunhagen, T., et al., *Intervertebral disk nutrition: A review of factors influencing concentrations of nutrients and metabolites.* Orthopedic Clinics of North America, 2011. **42**(4): p. 465.

12. Neidlinger-Wilke, C., et al., *Interactions of environmental conditions and mechanical loads have influence on matrix turnover by nucleus pulposus cells.* Journal of Orthopaedic Research, 2012. **30**(1): p. 112-121.

13. Zhou, S., Z. Cui, and J.P.G. Urban, *Nutrient gradients in engineered cartilage: Metabolic kinetics measurement and mass transfer modeling.* Biotechnology and Bioengineering, 2008. **101**(2): p. 408-421.

94

14.   Bibby, S.R.S., et al., *Metabolism of the intervertebral disc: Effects of low levels of oxygen, glucose, and pH on rates of energy metabolism of bovine nucleus pulposus cells.* Spine, 2005. **30**(5): p. 487-496.

15.   Grunhagen, T., et al., *Nutrient supply and intervertebral disc metabolism.* Journal of Bone and Joint Surgery-American Volume, 2006. **88a**: p. 30-35.

16.   An, H.S., et al., *Introduction - Disc degeneration: Summary.* Spine, 2004. **29**(23): p. 2677-2678.

17.   Huang, Y.C., J.P.G. Urban, and K.D.K. Luk, *OPINION Intervertebral disc regeneration: do nutrients lead the way?* Nature Reviews Rheumatology, 2014. **10**(9): p. 561-566.

18.   An, H.S., et al., *Introduction: disc degeneration: summary.* Spine (Phila Pa 1976), 2004. **29**(23): p. 2677-8.

19.   Urban, J.P.G., S. Smith, and J.C.T. Fairbank, *Nutrition of the intervertebral disc.* Spine, 2004. **29**(23): p. 2700-2709.

20.   Wu, Y.R., et al., *Effect of cartilage endplate on cell based disc regeneration: A finite element analysis.* Molecular & Cellular Biomechanics, 2013. **10**(2): p. 159-182.

21.   Jackson, A.R., C.Y. Huang, and W.Y. Gu, *Effect of endplate calcification and mechanical deformation on the distribution of glucose in intervertebral disc: a 3D finite element study.* Computer Methods in Biomechanics and Biomedical Engineering, 2011. **14**(2): p. 195-204.

22.   Gonzales, S., et al., *Measurement of ATP-induced membrane potential changes in IVD cells.* Cellular and Molecular Bioengineering, 2014. **7**(4): p. 598-606.

23.   Hirschberg, C.B., P.W. Robbins, and C. Abeijon, *Transporters of nucleotide sugars, ATP, and nucleotide sulfate in the endoplasmic reticulum and Golgi apparatus.* Annual Review of Biochemistry, 1998. **67**: p. 49-69.

24.   Prydz, K. and K.T. Dalen, *Synthesis and sorting of proteoglycans - Commentary.* Journal of Cell Science, 2000. **113**(2): p. 193-205.

25.   Burnstock, G., *The past, present and future of purine nucleotides as signalling molecules.* Neuropharmacology, 1997. **36**(9): p. 1127-1139.

26.   Croucher, L.J., et al., *Extracellular ATP and UTP stimulate cartilage proteoglycan and collagen accumulation in bovine articular chondrocyte pellet cultures.* Biochimica Et Biophysica Acta-Molecular Basis of Disease, 2000. **1502**(2): p. 297-306.

27. Waldman, S.D., et al., *Harnessing the purinergic receptor pathway to develop functional engineered cartilage constructs.* Osteoarthritis and Cartilage, 2010. **18**(6): p. 864-872.

28. Wang, C., et al., *Energy metabolism of intervertebral disc under mechanical loading.* Journal of Orthopaedic Research, 2013. **31**(11): p. 1733-1738.

29. Gonzales, S., et al., *ATP promotes extracellular matrix biosynthesis of intervertebral disc cells.* Cell and Tissue Research, 2015. **359**(2): p. 635-642.

30. Pickup, J. and H. Keen, *Continuous subcutaneous insulin infusion at 25 years - Evidence base for the expanding use of insulin pump therapy in type 1 diabetes.* Diabetes Care, 2002. **25**(3): p. 593-598.

31. Clark, W.R., *Hemodialyzer membranes and configurations: a historical perspective.* Semin Dial, 2000. **13**(5): p. 309-11.

32. Ettenson, D.S. and E.R. Edelman, *Local drug delivery: an emerging approach in the treatment of restenosis.* Vascular Medicine, 2000. **5**(2): p. 97-102.

33. Bidros, D.S. and M.A. Vogelbaum, *Novel drug delivery strategies in neuro-oncology.* Neurotherapeutics, 2009. **6**(3): p. 539-546.

34. Bron, J.L., et al., *Biomechanical and in vivo evaluation of experimental closure devices of the annulus fibrosus designed for a goat nucleus replacement model.* European Spine Journal, 2010. **19**(8): p. 1347-1355.

35. Likhitpanichkul, M., et al., *Fibrin-genipin adhesive hydrogel for annulus fibrosus repair: performance evaluation with large animal organ culture, in situ biomechanics, and in vivo degradation tests.* European Cells & Materials, 2014. **28**: p. 25-38.

36. Long, R.G., et al., *In vitro and biomechanical screening of polyethylene glycol and poly(trimethylene carbonate) block copolymers for annulus fibrosus repair.* J Tissue Eng Regen Med, 2016.

37. Yang, X.L. and X.D. Li, *Nucleus pulposus tissue engineering: a brief review.* European Spine Journal, 2009. **18**(11): p. 1564-1572.

38. Chik, T.K., et al., *Photochemically crosslinked collagen annulus plug: a potential solution solving the leakage problem of cell-based therapies for disc degeneration.* Acta Biomater, 2013. **9**(9): p. 8128-39.

39. Guiot, B.H. and R.G. Fessler, *Molecular biology of degenerative disc disease.* Neurosurgery, 2000. **47**(5): p. 1034-1040.

40. Masuda, K. and J.C. Lotz, *New challenges for intervertebral disc treatment using regenerative medicine.* Tissue Engineering Part B-Reviews, 2010. **16**(1): p. 147-158.

41. Erwin, W.M. and K.E. Hood, *The cellular and molecular biology of the intervertebral disc: A clinician's primer.* J Can Chiropr Assoc, 2014. **58**(3): p. 246-57.

42. Ombregt, L., *A System of Orthopaedic Medicine (Third Edition).* 2013: Churchill Livingstone, Elsevier.

43. Kandel, R., S. Roberts, and J.P.G. Urban, *Tissue engineering and the intervertebral disc: the challenges.* European Spine Journal, 2008. **17**: p. S480-S491.

44. Hu, J.G., et al., *Injectable silk fibroin/polyurethane composite hydrogel for nucleus pulposus replacement.* Journal of Materials Science-Materials in Medicine, 2012. **23**(3): p. 711-722.

45. Roberts, S., et al., *Histology and pathology of the human intervertebral disc.* Journal of Bone and Joint Surgery-American Volume, 2006. **88a**: p. 10-14.

46. Gantenbein, B., et al., *Activation of intervertebral disc cells by co-culture with notochordal cells, conditioned medium and hypoxia.* Bmc Musculoskeletal Disorders, 2014. **15**.

47. Aguiar, D.J., S.L. Johnson, and T.R. Oegema, *Notochordal cells interact with nucleus pulposus cells: Regulation of proteoglycan synthesis.* Experimental Cell Research, 1999. **246**(1): p. 129-137.

48. Guehring, T., et al., *Notochordal intervertebral disc cells sensitivity to nutrient deprivation.* Arthritis and Rheumatism, 2009. **60**(4): p. 1026-1034.

49. Roughley, P.J., *Biology of intervertebral disc aging and degeneration - Involvement of the extracellular matrix.* Spine, 2004. **29**(23): p. 2691-2699.

50. Paesold, G., A.G. Nerlich, and N. Boos, *Biological treatment strategies for disc degeneration: potentials and shortcomings.* European Spine Journal, 2007. **16**(4): p. 447-468.

51. MacGregor, A.J., et al., *Structural, psychological, and genetic influences on low back and neck pain: A study of adult female twins.* Arthritis & Rheumatism-Arthritis Care & Research, 2004. **51**(2): p. 160-167.

52. Battie, M.C. and T. Videman, *Lumbar disc degeneration: Epidemiology and genetics.* Journal of Bone and Joint Surgery-American Volume, 2006. **88a**: p. 3-9.

53.   Ogata, K. and L.A. Whiteside, *1980 Volvo award winner in basic science. Nutritional pathways of the intervertebral disc. An experimental study using hydrogen washout technique.* Spine (Phila Pa 1976), 1981. **6**(3): p. 211-6.

54.   Rajasekaran, S., et al., *ISSLS prize winner: A study of diffusion in human lumbar discs: A serial magnetic resonance imaging study documenting the influence of the endplate on diffusion in normal and degenerate discs.* Spine, 2004. **29**(23): p. 2654-2667.

55.   Miller, J.A., C. Schmatz, and A.B. Schultz, *Lumbar disc degeneration: correlation with age, sex, and spine level in 600 autopsy specimens.* Spine (Phila Pa 1976), 1988. **13**(2): p. 173-8.

56.   Nerlich, A.G., E.D. Schleicher, and N. Boos, *1997 Volvo Award winner in basic science studies - Immunohistologic markers for age-related changes of human lumbar intervertebral discs.* Spine, 1997. **22**(24): p. 2781-2795.

57.   Drazin, D., et al., *Stem cell therapy for degenerative disc disease.* Adv Orthop, 2012. **2012**: p. 961052.

58.   Fritzell, P., et al., *2001 Volvo Award winner in clinical studies: Lumbar fusion versus nonsurgical treatment for chronic low back pain - A multicenter randomized controlled trial from the Swedish Lumbar Spine Study Group.* Spine, 2001. **26**(23): p. 2521-2532.

59.   Schizas, C., G. Kulik, and V. Kosmopoulos, *Disc degeneration: current surgical options.* European Cells & Materials, 2010. **20**: p. 306-315.

60.   Wagner, W.H., et al., *Access strategies for revision or explantation of the Charite lumbar artificial disc replacement.* Journal of Vascular Surgery, 2006. **44**(6): p. 1266-1272.

61.   Masuda, K., *Biological repair of the degenerated intervertebral disc by the injection of growth factors.* European Spine Journal, 2008. **17**: p. S441-S451.

62.   Masuda, K., T.R. Oegema, and H.S. An, *Growth factors and treatment of intervertebral disc degeneration.* Spine, 2004. **29**(23): p. 2757-2769.

63.   Osada, R., et al., *Autocrine/paracrine mechanism of insulin-like growth factor-1 secretion, and the effect of insulin-like growth factor-1 on proteoglycan synthesis in bovine intervertebral discs.* Journal of Orthopaedic Research, 1996. **14**(5): p. 690-699.

64.   Thompson, J.P., T.R. Oegema, Jr., and D.S. Bradford, *Stimulation of mature canine intervertebral disc by growth factors.* Spine (Phila Pa 1976), 1991. **16**(3): p. 253-60.

65.   Walsh, A.J.L., D.S. Bradford, and J.C. Lotz, *In vivo growth factor treatment of degenerated intervertebral discs.* Spine, 2004. **29**(2): p. 156-163.

66.   Pratsinis, H. and D. Kletsas, *PDGF, bFGF and IGF-I stimulate the proliferation of intervertebral disc cells in vitro via the activation of the ERK and Akt signaling pathways.* European Spine Journal, 2007. **16**(11): p. 1858-1866.

67.   Barthmes, M., et al., *Electrophysiological characterization of the ATP-ADP translocase in native mitochondrial membranes.* Biophysical Journal, 2013. **104**(2): p. 629a-629a.

68.   Knowles, J.R., *Enzyme-catalyzed phosphoryl transfer-reactions.* Annual Review of Biochemistry, 1980. **49**: p. 877-919.

69.   Grad, S., et al., *The use of biodegradable polyurethane scaffolds for cartilage tissue engineering: potential and limitations.* Biomaterials, 2003. **24**(28): p. 5163-5171.

70.   Asefnejad, A., et al., *Manufacturing of biodegradable polyurethane scaffolds based on polycaprolactone using a phase separation method: physical properties and in vitro assay.* International Journal of Nanomedicine, 2011. **6**: p. 2375-2384.

71.   Hu, Z.J., et al., *The in vivo performance of small-caliber nanofibrous polyurethane vascular grafts.* Bmc Cardiovascular Disorders, 2012. **12**.

72.   Tsui, Y.K. and S. Gogolewski, *Microporous biodegradable polyurethane membranes for tissue engineering.* Journal of Materials Science-Materials in Medicine, 2009. **20**(8): p. 1729-1741.

73.   Xu, W.L., et al., *Mechanical properties of small-diameter polyurethane vascular grafts reinforced by weft-knitted tubular fabric.* Journal of Biomedical Materials Research Part A, 2010. **92A**(1): p. 1-8.

74.   Wang, H.Y., et al., *Co-electrospun blends of PU and PEG as potential biocompatible scaffolds for small-diameter vascular tissue engineering.* Materials Science & Engineering C-Materials for Biological Applications, 2012. **32**(8): p. 2306-2315.

75.   Khorasani, M.T. and S. Shorgashti, *Fabrication of microporous inversion method as small material polyurethane by spray phase diameter vascular grafts.* Journal of Biomedical Materials Research Part A, 2006. **77A**(2): p. 253-260.

76.   Whatley, B.R., et al., *Fabrication of a biomimetic elastic intervertebral disk scaffold using additive manufacturing.* Biofabrication, 2011. **3**(1).

77.   Hung, K.C., C.S. Tseng, and S.H. Hsu, *Synthesis and 3D printing of biodegradable polyurethane elastomer by a water-based process for cartilage tissue engineering applications.* Advanced Healthcare Materials, 2014. **3**(10): p. 1578-1587.

78.   Gorna, K. and S. Gogolewski, *Biodegradable porous polyurethane scaffolds for tissue repair and regeneration.* Journal of Biomedical Materials Research Part A, 2006. **79A**(1): p. 128-138.

79.   Heijkants, R.G.J.C., et al., *Polyurethane scaffold formation via a combination of salt leaching and thermally induced phase separation.* Journal of Biomedical Materials Research Part A, 2008. **87A**(4): p. 921-932.

80.   Levene, H.B., *Analysis of tyrosine-derived novel synthetic polymer scaffold devices for guided tissue regeneration.* 1999, Rutgers University and the University of Medicine and Dentistry of New Jersey: New Brunswick, NJ. p. 167.

81.   Gupta, B., S. Patra, and A.R. Ray, *Preparation of porous polycaprolactone tubular matrix by salt leaching process.* Journal of Applied Polymer Science, 2012. **126**(5): p. 1505-1510.

82.   Hollister, S.J., *Porous scaffold design for tissue engineering.* Nature Materials, 2005. **4**(7): p. 518-524.

83.   Stylianopoulos, T., et al., *Computational predictions of the tensile properties of electrospun fibre meshes: Effect of fibre diameter and fibre orientation.* Journal of the Mechanical Behavior of Biomedical Materials, 2008. **1**(4): p. 326-335.

84.   Hayashi, K., et al., *Elastic properties and strength of a novel small-diameter, compliant polyurethane vascular graft.* Journal of Biomedical Materials Research-Applied Biomaterials, 1989. **23**(A2): p. 229-244.

85.   Khorasani, M.T. and S. Shorgashti, *Fabrication of microporous thermoplastic polyurethane for use as small-diameter vascular graft material. I. Phase-inversion method.* Journal of Biomedical Materials Research Part B-Applied Biomaterials, 2006. **76B**(1): p. 41-48.

86.   Hutmacher, D.W., *Scaffold design and fabrication technologies for engineering tissues - state of the art and future perspectives.* Journal of Biomaterials Science-Polymer Edition, 2001. **12**(1): p. 107-124.

87.   Heijkants, R.G.J.C., et al., *Preparation of a polyurethane scaffold for tissue engineering made by a combination of salt leaching and freeze-drying of dioxane.* Journal of Materials Science, 2006. **41**(8): p. 2423-2428.

88. Tsai, M.C., et al., *Evaluation of biodegradable elastic scaffolds made of anionic polyurethane for cartilage tissue engineering.* Colloids and Surfaces B-Biointerfaces, 2015. **125**: p. 34-44.

89. Bil, M., J. Ryszkowska, and K.J. Kurzydlowski, *Effect of polyurethane composition and the fabrication process on scaffold properties.* Journal of Materials Science, 2009. **44**(6): p. 1469-1476.

90. Gogolewski, S., et al., *Structure-property relations and cytotoxicity of isosorbide-based biodegradable polyurethane scaffolds for tissue repair and regeneration.* Journal of Biomedical Materials Research Part A, 2008. **85A**(2): p. 456-465.

91. Yuan, T.Y., et al., *Strain-dependent oxygen diffusivity in bovine annulus fibrosus.* Journal of Biomechanical Engineering-Transactions of the Asme, 2009. **131**(7).

92. Jackson, A.R., et al., *Effect of compression and anisotropy on the diffusion of glucose in annulus fibrosus.* Spine, 2008. **33**(1): p. 1-7.

93. Jackson, A.R. and W.Y. Gu, *Transport properties of cartilaginous tissues.* Current Rheumatology Review, 2009. **5**(1): p. 40-50.

94. Kang, H., C.Y. Lin, and S.J. Hollister, *Topology optimization of three dimensional tissue engineering scaffold architectures for prescribed bulk modulus and diffusivity.* Structural and Multidisciplinary Optimization, 2010. **42**(4): p. 633-644.

95. Jones, A.C., et al., *The correlation of pore morphology, interconnectivity and physical properties of 3D ceramic scaffolds with bone ingrowth.* Biomaterials, 2009. **30**(7): p. 1440-1451.

96. Jones, A.C., et al., *Assessment of bone ingrowth into porous biomaterials using MICRO-CT.* Biomaterials, 2007. **28**(15): p. 2491-2504.

97. Boccaccini, A.R. and Z. Fan, *A new approach for the Young's modulus-porosity correlation of ceramic materials.* Ceramics International, 1997. **23**(3): p. 239-245.

98. Chen, Q., et al., *Modelling of the strength-porosity relationship in glass-ceramic foam scaffolds for bone repair.* Journal of the European Ceramic Society, 2014. **34**(11): p. 2663-2673.

99. Gibson, L.J., *Biomechanics of cellular solids.* J Biomech, 2005. **38**(3): p. 377-99.

100. Harley, B.A., et al., *Mechanical characterization of collagen-glycoaminoglycan scaffolds.* Acta Biomaterialia, 2007. **3**: p. 463-474.

101. Kanungo, B.P. and L.J. Gibson, *Density-property relationships in collagen-glycosaminoglycan scaffolds.* Acta Biomater, 2010. **6**(2): p. 344-53.

102.   Chen, J.H., et al., *Microporous segmented polyetherurethane vascular graft: I. Dependency of graft morphology and mechanical properties on compositions and fabrication conditions.* Journal of Biomedical Materials Research, 1999. **48**(3): p. 235-245.

103.   lewis, H.D., K.L. Walters, and K.A. Johnson, *Particle size distribution by area analysis: modifications and extensions of the saltykov method.* Metallography, 1973. **6**(2): p. 93-101.

104.   Shen, H., et al., *Numerical modeling of pore size and distribution in foamed titanium.* Mechanics of Materials, 2006. **38**(8-10): p. 933-944.

105.   Yuan, T.Y., C.Y. Huang, and W.Y. Gu, *Novel technique for Online characterization of cartilaginous tissue properties.* Journal of Biomechanical Engineering-Transactions of the Asme, 2011. **133**(9).

106.   Gao, X. and W.Y. Gu, *A new constitutive model for hydration-dependent mechanical properties in biological soft tissues and hydrogels.* Journal of Biomechanics, 2014. **47**(12): p. 3196-3200.

107.   Gu, W.Y., et al., *New insight into deformation-dependent hydraulic permeability of gels and cartilage, and dynamic behavior of agarose gels in confined compression.* Journal of Biomechanics, 2003. **36**(4): p. 593-598.

108.   Jackson, A.R., et al., *Nutrient transport in human annulus fibrosus is affected by compressive strain and anisotropy.* Annals of Biomedical Engineering, 2012. **40**(12): p. 2551-2558.

109.   Wang, C., C.Y.C. Huang, and W.C. Lin, *Optical ATP biosensor for extracellular ATP measurement.* Biosensors & Bioelectronics, 2013. **43**: p. 355-361.

110.   Gu, W.Y., et al., *Diffusivity of ions in agarose gels and intervertebral disc: Effect of porosity.* Annals of Biomedical Engineering, 2004. **32**(12): p. 1710-1717.

111.   Hillsley, M.V. and J.A. Frangos, *Bone tissue engineering: the role of interstitial fluid flow.* Biotechnol Bioeng, 1994. **43**(7): p. 573-81.

112.   Agrawal, C.M., et al., *Effects of fluid flow on the in vitro degradation kinetics of biodegradable scaffolds for tissue engineering.* Biomaterials, 2000. **21**(23): p. 2443-52.

113.   Weyand, B., et al., *A differential pressure laminar flow reactor supports osteogenic differentiation and extracellular matrix formation from adipose mesenchymal stem cells in a macroporous ceramic scaffold.* Biores Open Access, 2012. **1**(3): p. 145-56.

114. Gemmiti, C.V. and R.E. Guldberg, *Fluid flow increases type II collagen deposition and tensile mechanical properties in bioreactor-grown tissue-engineered cartilage.* Tissue Eng, 2006. **12**(3): p. 469-79.

115. Correia, C., et al., *Dynamic culturing of cartilage tissue: the significance of hydrostatic pressure.* Tissue Eng Part A, 2012. **18**(19-20): p. 1979-91.

116. Dias, M.R., et al., *Permeability analysis of scaffolds for bone tissue engineering.* Journal of Biomechanics, 2012. **45**(6): p. 938-944.

117. Woo Jung, J., et al., *Evaluation of the effective diffusivity of a freeform fabricated scaffold using computational simulation.* J Biomech Eng, 2013. **135**(8): p. 84501.

118. Karande, T.S., J.L. Ong, and C.M. Agrawal, *Diffusion in musculoskeletal tissue engineering scaffolds: design issues related to porosity, permeability, architecture, and nutrient mixing.* Ann Biomed Eng, 2004. **32**(12): p. 1728-43.

119. Dawson, M.A., J.T. Germaine, and L.J. Gibson, *Permeability of open-cell foams under compressive strain.* International Journal of Solids and Structures, 2007. **44**(16): p. 5133-5145.

120. O'Brien, F.J., et al., *The effect of pore size on permeability and cell attachment in collagen scaffolds for tissue engineering.* Technol Health Care, 2007. **15**(1): p. 3-17.

121. Mitsak, A.G., et al., *Effect of polycaprolactone scaffold permeability on bone regeneration in vivo.* Tissue Engineering Part A, 2011. **17**(13-14): p. 1831-1839.

122. Albro, M.B., et al., *Dynamic loading of deformable porous media can induce active solute transport.* Journal of Biomechanics, 2008. **41**(15): p. 3152-3157.

123. Huang, C.Y. and W.Y. Gu, *Effects of tension-compression nonlinearity on solute transport in charged hydrated fibrous tissues under dynamic unconfined compression.* J Biomech Eng, 2007. **129**(3): p. 423-9.

124. Carter, D.R. and W.C. Hayes, *The compressive behavior of bone as a two-phase porous structure.* J Bone Joint Surg Am, 1977. **59**(7): p. 954-62.

125. Karageorgiou, V. and D. Kaplan, *Porosity of 3D biomaterial scaffolds and osteogenesis.* Biomaterials, 2005. **26**(27): p. 5474-91.

126. Sin, D., et al., *Polyurethane (PU) scaffolds prepared by solvent casting/particulate leaching (SCPL) combined with centrifugation.* Materials Science & Engineering C-Materials for Biological Applications, 2010. **30**(1): p. 78-85.

127. Costa, A., *Permeability-porosity relationship: A reexamination of the Kozeny-Carman equation based on a fractal pore-space geometry assumption.* Geophysical Research Letters, 2006. **33**(2).

128. Long, R.G., et al., *Design requirements for annulus fibrosus repair: review of forces, displacements, and material properties of the intervertebral disk and a summary of candidate hydrogels for repair.* Journal of Biomechanical Engineering-Transactions of the Asme, 2016. **138**(2).

129. Wang, Y.F., et al., *Systematic characterization of porosity and mass transport and mechanical properties of porous polyurethane scaffolds.* J Mech Behav Biomed Mater, 2016. **65**: p. 657-664.

130. Huang, C.Y.C., M.A. Deitzer, and H.S. Cheung, *Effects of fibrinolytic inhibitors on chondrogenesis of bone-marrow derived mesenchymal stem cells in fibrin gels.* Biomechanics and Modeling in Mechanobiology, 2007. **6**(1-2): p. 5-11.

131. Yao, H., et al., *Effects of swelling pressure and hydraulic permeability on dynamic compressive behavior of lumbar annulus fibrosus.* Annals of Biomedical Engineering, 2002. **30**(10): p. 1234-1241.

132. Johnson, S. and P. Rabinovitch, *Ex vivo imaging of excised tissue using vital dyes and confocal microscopy.* Curr Protoc Cytom, 2012. **Chapter 9**: p. Unit 9 39.

133. Chida, J., et al., *An efficient extraction method for quantitation of adenosine triphosphate in mammalian tissues and cells.* Analytica Chimica Acta, 2012. **727**: p. 8-12.

134. Fernando, H.N., et al., *Mechanical loading affects the energy metabolism of intervertebral disc cells.* J Orthop Res, 2011. **29**(11): p. 1634-41.

135. Martin, J.A., et al., *Mitochondrial electron transport and glycolysis are coupled in articular cartilage.* Osteoarthritis and Cartilage, 2012. **20**(4): p. 323-329.

136. Johnson, K., et al., *Mitochondrial oxidative phosphorylation is a downstream regulator of nitric oxide effects on chondrocyte matrix synthesis and mineralization.* Arthritis and Rheumatism, 2000. **43**(7): p. 1560-1570.

137. Johnson, K., et al., *Mediation of spontaneous knee osteoarthritis by progressive chondrocyte ATP depletion in Hartley guinea pigs.* Arthritis and Rheumatism, 2004. **50**(4): p. 1216-1225.

138. Elliott, D.M., et al., *The effect of relative needle diameter in puncture and sham injection animal models of degeneration.* Spine (Phila Pa 1976), 2008. **33**(6): p. 588-96.

139.   Hsieh, A.H., et al., *Degenerative anular changes induced by puncture are associated with insufficiency of disc biomechanical function.* Spine, 2009. **34**(10): p. 998-1005.

140.   Sobajima, S., et al., *A slowly progressive and reproducible animal model of intervertebral disc degeneration characterized by MRI, x-ray, and histology.* Spine, 2005. **30**(1): p. 15-24.

141.   Korecki, C.L., J.J. Costi, and J.C. Iatridis, *Needle puncture injury affects intervertebral disc mechanics and biology in an organ culture model.* Spine, 2008. **33**(3): p. 235-241.

142.   MacLean, J.J., et al., *Effects of immobilization and dynamic compression on intervertebral disc cell gene expression in vivo.* Spine, 2003. **28**(10): p. 973-981.

143.   Walter, B.A., et al., *Complex loading affects intervertebral disc mechanics and biology.* Osteoarthritis Cartilage, 2011. **19**(8): p. 1011-8.

144.   Wang, D.L., S.D. Jiang, and L.Y. Dai, *Biologic response of the intervertebral disc to static and dynamic compression in vitro.* Spine (Phila Pa 1976), 2007. **32**(23): p. 2521-8.

145.   Gu, W.Y. and H. Yao, *Effects of hydration and fixed charge density on fluid transport in charged hydrated soft tissues.* Annals of Biomedical Engineering, 2003. **31**(10): p. 1162-1170.

146.   Michalek, A.J., et al., *The effects of needle puncture injury on microscale shear strain in the intervertebral disc annulus fibrosus.* Spine Journal, 2010. **10**(12): p. 1098-1105.

147.   Huang, C.Y. and W.Y. Gu, *Effects of mechanical compression on metabolism and distribution of oxygen and lactate in intervertebral disc.* Journal of Biomechanics, 2008. **41**(6): p. 1184-1196.

148.   Acosta, F.L., et al., *Porcine intervertebral disc repair using allogeneic juvenile articular chondrocytes or mesenchymal stem cells.* Tissue Engineering Part A, 2011. **17**(23-24): p. 3045-3055.

149.   Henriksson, H.B., et al., *Transplantation of human mesenchymal stems cells into intervertebral discs in a xenogeneic porcine model.* Spine, 2009. **34**(2): p. 141-148.

150.   Feng, G.J., et al., *Transplantation of mesenchymal stem cells and nucleus pulposus cells in a degenerative disc model in rabbits: a comparison of 2 cell types as potential candidates for disc regeneration Laboratory investigation.* Journal of Neurosurgery-Spine, 2011. **14**(3): p. 322-329.

151.   Schmidt, H., et al., *Response analysis of the lumbar spine during regular daily activities--a finite element analysis.* J Biomech, 2010. **43**(10): p. 1849-56.

152.   Im, M.J.C., M.F. Freshwater, and J.E. Hoopes, *Enzyme-activities in granulation tissue - energy for collagen-synthesis.* Journal of Surgical Research, 1976. **20**(2): p. 121-125.

153.   Lee, R.B. and J.P. Urban, *Evidence for a negative Pasteur effect in articular cartilage.* Biochem J, 1997. **321 (Pt 1)**: p. 95-102.

154.   Baker, M.S., J. Feigan, and D.A. Lowther, *The mechanism of chondrocyte hydrogen-peroxide damage - depletion of intracellular ATP due to suppression of glycolysis caused by oxidation of glyceraldehyde-3-phosphate dehydrogenase.* Journal of Rheumatology, 1989. **16**(1): p. 7-14.

155.   Bibby, S.R. and J.P. Urban, *Effect of nutrient deprivation on the viability of intervertebral disc cells.* Eur Spine J, 2004. **13**(8): p. 695-701.

156.   Lai, W.M., J.S. Hou, and V.C. Mow, *A triphasic theory for the swelling and deformation behaviors of articular-cartilage.* Journal of Biomechanical Engineering-Transactions of the Asme, 1991. **113**(3): p. 245-258.

157.   Yao, H. and W.Y. Gu, *Physical signals and solute transport in human intervertebral disc during compressive stress relaxation: 3D finite element analysis.* Biorheology, 2006. **43**(3-4): p. 323-335.

158.   Yao, H. and W.Y. Gu, *Three-dimensional inhomogeneous triphasic finite-element analysis of physical signals and solute transport in human intervertebral disc under axial compression.* Journal of Biomechanics, 2007. **40**(9): p. 2071-2077.

159.   Huang, C.Y., F. Travascio, and W.Y. Gu, *Quantitative analysis of exogenous IGF-1 administration of intervertebral disc through intradiscal injection.* J Biomech, 2012. **45**(7): p. 1149-55.

160.   Guehring, T., et al., *Notochordal intervertebral disc cells: sensitivity to nutrient deprivation.* Arthritis Rheum, 2009. **60**(4): p. 1026-34.

161.   Jackson, A.R., *Transport and Metabolism of Glucose in Intervertebral Disc.* Open Access Dissertations. 479, 2010.

162.   Soukane, D.M., A. Shirazi-Adl, and J.P. Urban, *Analysis of nonlinear coupled diffusion of oxygen and lactic acid in intervertebral discs.* J Biomech Eng, 2005. **127**(7): p. 1121-6.

163.   Li, W., et al., *The dependency of solute diffusion on molecular weight and shape in intact bone.* Bone, 2009. **45**(5): p. 1017-1023.

164. Fazzalari, N.L., et al., *Antero-postero differences in cortical thickness and cortical porosity of T12 to L5 vertebral bodies.* Joint Bone Spine, 2006. **73**(3): p. 293-7.

165. Doblare, M., J.M. Garcia, and M.J. Gomez, *Modelling bone tissue fracture and healing: a review.* Engineering Fracture Mechanics, 2004. **71**(13-14): p. 1809-1840.

166. Hussain, M., et al., *Relationship between biomechanical changes at adjacent segments and number of fused bone grafts in multilevel cervical fusions: a finite element investigation Technical note.* Journal of Neurosurgery-Spine, 2014. **20**(1): p. 22-29.

167. Gu, W.Y., H. Yao, and A.L. Vega, *Effect of water volume fraction on electrical conductivity and ion diffusivity in agarose gels.* IUTAM Symposium on Physicochemical and Electromechanical Interactions in Porous Media, 2005. **125**: p. 193-199.

168. Holm, S., G. Selstam, and A. Nachemson, *Carbohydrate-metabolism and concentration profiles of solutes in the canine lumbar intervertebral-disk.* Acta Physiologica Scandinavica, 1982. **115**(1): p. 147-156.

169. Ishihara, H. and J.P. Urban, *Effects of low oxygen concentrations and metabolic inhibitors on proteoglycan and protein synthesis rates in the intervertebral disc.* J Orthop Res, 1999. **17**(6): p. 829-35.

170. Huang, C.Y., et al., *Effects of low glucose concentrations on oxygen consumption rates of intervertebral disc cells.* Spine (Phila Pa 1976), 2007. **32**(19): p. 2063-9.